Utrecht University

Faculty of Physics and Astronomy

Dynamics of sandbars in the nearshore zone of coastal seas: the role of time dependent angle of wave incidence

Bachelor Thesis

Niek van Andel

Supervisors:

Prof. Dr. H.E. de Swart
Institute for Marine and Atmospheric Research (IMAU)

Dr. A. Nnafie
Institute for Marine and Atmospheric Research (IMAU)

June 13, 2018

Abstract

Knowledge about sandbars in the surf zone of coastal seas (the zone where waves break), is of great importance in order to preserve beach stability and therefore beach safety. In channels between sandbars namely, strong seaward directed currents are observed: rip currents. These currents arise due to alongshore variations in sea level, resulting from differential intensities of wave breaking at sandbars and channels in between them.
In recent years, nonlinear hydrodynamic models have been developed to analyse the formation of sandbars and rip currents, for different types of coast and wave forcing. In these models, rips also drive the formation of sandbars, as they cause convergence of sediment transport in bar areas. The characteristics of sandbars vary with the angle of wave incidence and the use of periodically varying wave angles results in different behaviour than the use of a constant wave angle. The main new aspect of the present study is that this periodic wave forcing is not necessarily limited to a mean wave angle normal to the coast.
Results show that for periodically varying wave forcing with on average normal wave incidence, the mean height of the sandbars is not equal to that of sandbars for constant normal incoming waves and moreover depends on the amplitude and period of the time varying wave forcing. Overall, the response of the system depends on the rate of change of wave angle, compared to the time at which the system adapts to a change in wave angle. For periodically varying angles of wave incidence with non zero mean, the response is more complex and not fully understood. The specific details therefore deserve further attention in the near future.

Front page: Wave breaking pattern at the Dutch coast near Hoek van Holland. At the coast line itself all waves break, but somewhat offshore, an irregular wave breaking pattern appears, possibly due to the presence of rip channels. Photo taken on December 19th 2014, own archive.

Layman summary (Dutch)

In dit onderzoek is gekeken naar de formatie en het gedrag van zandbanken en stromingen in de kustzone voor kusten vergelijkbaar met de Nederlandse Noordzeekust of the Franse Atlantische kust nabij Biskaje. Vooral in de zomermaanden is het een punt van zorg dat de kustafwaartse stromingen tussen de zandbanken de zwemveiligheid beperken. Door deze muistromingen moeten reddingsbrigades in heel Nederland alleen al honderden keren uitrukken voor zwemmers die hierdoor in problemen zijn gekomen. Het precieze gedrag van deze zandbanken en muistromingen is dus van groot belang voor de veiligheid, maar ook voor de stabiliteit van de kust. Echter, kennis over de grootte van deze zandbanken is slechts beperkt.

Modelstudies hebben het gedrag van zandbanken voor de kust onderzocht in gevallen dat golven voor lange tijd loodrecht of juist met een schuine hoek het strand naderen. In realiteit verandert de golfrichting van tijd tot tijd, waardoor een keuze voor een constante golfinval niet altijd even realistisch is. Daarom is in dit onderzoek gekozen voor een variërende hoek van inval. Het gemiddelde van deze variatie is niet alleen loodrecht op de kust gekozen, maar ook zo dat gemiddeld over de tijd de golven schuin invallen. In de Noordzee bijvoorbeeld is de dominerende golfrichting namelijk niet west-oost georiënteerd, maar komen de golven uit het noord-of zuidwesten, ofwel, gemiddeld schuin ten opzichte van de kust.

Een belangrijk resultaat van deze studie is dat een afwijkend gedrag van de zandbanken gevonden is vergeleken met constante golfcondities. Het blijkt dat de zandbanken een bepaalde tijd nodig hebben om zich aan te kunnen passen aan een nieuwe golfrichting. Als de golfrichting snel verandert, dan hebben de zandbanken geen tijd om zich aan te passen en blijft het effect van de variatie beperkt. Als variaties daarentegen zeer langzaam zijn, kan het systeem van zandbanken zich aanpassen aan de nieuwe situatie en lijken de resultaten meer op resultaten van constante golfcondities. Als de aanpassingstijd van de zandbanken echter ongeveer gelijk is met de tijd van de opgelegde verandering, kunnen zandbanken hoger worden dan bij een constante hoek van inval het geval is. Daarnaast is in sommige gevallen zichtbaar dat zandbanken hun maximale hoogte bereiken op het moment dat de golven schuin op de kust afkomen, terwijl voor schuine invalshoeken juist lagere zandbanken ontstaan bij constante schuine invalshoek. Deze effecten verschillen echter als de variatie in golfrichting niet gemiddeld nul is en zijn complexer om te analyseren.

Voor vervolgonderzoek is het onder andere interessant om waargenomen golfcondities te gebruiken. In dat geval kunnen ook de golfhoogte en de golfperiode veranderen in tijd en hoeven veranderingen in niet altijd geleidelijk te verlopen.

Contents

1 Introduction

1.1 Coastal zone

Since the first human civilisations, settlements often have been built along the coast, mostly for strategic reasons such as defending mechanisms or trade opportunities. Nowadays, these reasons still hold and in addition, recreational opportunities can be seen as another reason that approximately half of the global population lives within 100 km of a coastline [*Davis Jr. and Fitzgerald*, 2004]. Of the total amount of 440.000 km of the world's coastline, 25% exists of sandy beaches [*Short*, 1999]. Knowledge about the complex, dynamic behaviour of the sandy beach systems therefore is important, e.g. to design engineering structures along the coast. Secondly, beach safety for recreational purposes can be improved if the dynamics of the beach are better understood. These sandy beach systems are morphological systems in the so-called nearshore zone, which is the area from the shoreline to the offshore region [*Davis Jr. and Fitzgerald*, 2004]. In this area, wave characteristics change because the waves experience differences in depth (shoaling zone), they ultimately break (surf zone) and finally they roll on to the beach (swash zone) [*Garnier*, 2006; *Ribas et al.*, 2015]. The different zones are shown in figure 1. The focus of this thesis is predominantly on features in the surf zone.

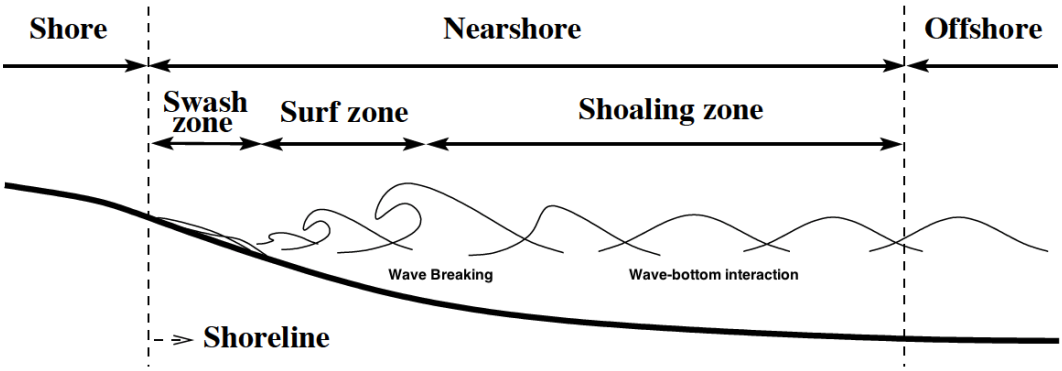

Figure 1: Overview of the coastal zone and different zones within. The focus of this thesis is predominantly on features in the surf zone. Figure modified after *Garnier* [2006].

1.2 Observations

Examples of a surf zone bottom pattern is that of crescentic bars [*Van Enckevort and Ruessink*, 2003], which consist of a periodic alongshore repetition of shoals and troughs. Often, the shoals are shaped in a way such that they form an undulating pattern in the horizontal plane. Since waves often break at these shoals, these patterns can be observed on satellite images as in figure 2. Systems of crescentic bars are also known for their strong offshore currents in the troughs, which bring swimmers into trouble and even cause several deadly incidents during the summer months, up to 100 in the United States every year [*Leatherman*, 2012]. These so-called rip currents make that the troughs in between sandbars

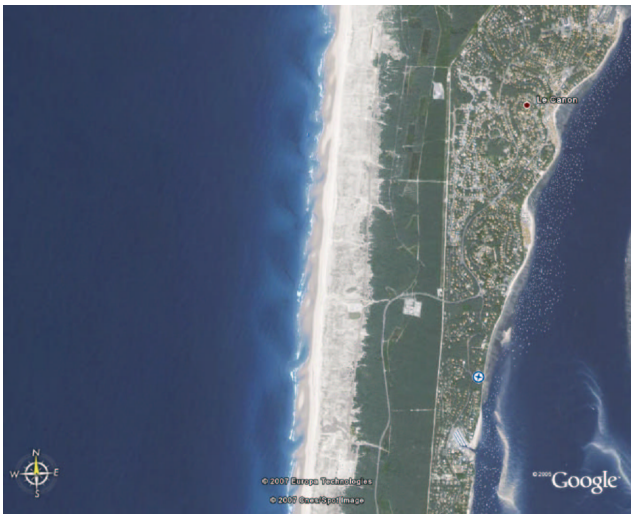

Figure 2: Crescentic bar patterns in front of the coast of Truc Vert, France. The patterns are recognised as the slightly lighter blue colour [*CoastalWiki*, 2017].

are called rip channels and often the entire system is called a rip channel system, instead of a system of crescentic bars [*Ribas et al.*, 2015]. The crescentic bars often form on top of an existing sandbar parallel to the coast [*Wright and Short*, 1984; *Garnier*, 2006]. After a storm event, at which all crescentic patterns vanish, it takes approximately 5-7 days for crescentic bars to form again and are typically observed for several days to weeks. [*Wright and Short*, 1984; *Lippmann and Holman*, 1990]. The most undulating patterns are found for wave conditions where the wave incidence is normal to the coast, the pattern straightens for more oblique angles of wave incidence. Besides, it is observed that the more oblique the wave incidence, the faster the bars migrate along the coast, with typically 10 m day^{-1} up to a maximum of 150 m day^{-1} [*Van Enckevort and Ruessink*, 2003].

1.3 Model studies

Not only observational studies have been done to the behaviour of such systems in the surf zone. Models have been developed to investigate the initial growth of these sandy beach systems [*Ribas et al.*, 2015]. To investigate the behaviour of the developed, mature sandbars, nonlinear models have been developed [*Garnier*, 2006; *Castelle and Ruessink*, 2011]. In these models, the growth of the sandbars decays in the course of time and sandbars obtain an almost constant height. The specific mechanisms causing this saturation have been investigated with these nonlinear models as well [*Garnier et al.*, 2006, 2010]. Also, phenomena as rip merging were observed [*Garnier et al.*, 2008, 2013; *Castelle and Ruessink*, 2011].
Waves are the main driver of the system in these model studies. Due to inherent flow (currents and waves)-topography interactions, instabilities can grow from which sandbars form. In most studies, this wave forcing has been held constant in time, either with a normal incidence or a oblique incidence. An exception is the study of *Castelle and Ruessink* [2011], in which periodic variations in wave height and wave period at normal incidence were imposed. Also, the direction of the wave incidence itself was periodically varied for several periods

and amplitudes of the variation, always with normal incidence on average. They showed that, despite the wave incidence was normal on average, the rip spacing and the mean height of the sandbars was affected, depending on the period and amplitude of the periodic variation.

1.4 Objective and outline

Obviously, in real physical situations, the average angle of wave incidence does not have to be 0°, i.e., normal to the coast [*Rutten et al.*, 2017]. Therefore, in this study, the main question to answer is: *"What are the characteristics of sandbar patterns under periodically varying wave conditions, where on average the waves are not only normal, but also oblique with respect to the coast?"* Since both constant oblique wave incidence as well as periodic changes were proven to have influence on the characteristics of bars and rip currents, it is hypothesized that the combination of these two causes different characteristics as well.

In order to answer the main question, the main objective is to produce and analyse experiments with periodically varying wave directions. To this end, the Morfo55 model developed by *Garnier* [2006], based on the Morfo50 model developed by *Caballeria et al.* [2002], is used, of which the details will be discussed in section 2. In section 3 the methodology to achieve this objective will be discussed. Results will be presented in section 4, followed by a discussion of these results in section 5 in which also the model limitations will be discussed and an outlook for further studies will be given. Finally in section 6, the conclusions will be formulated.

2 Model

2.1 Domain

The model that is used is the Morfo55 nonlinear model. The model focusses on the simulation of waves, currents and bottom evolution in the surf zone. Tides (an offshore feature) and beach modifications (located in the swash zone) are not included.
The model uses a Cartesian frame of reference of which a schematic view is shown in figure 3. The origin O is located at the coastline. The x-axis points in the offshore direction, with a seaward boundary at $x = L_x$. The y-axis points in the longshore direction, bounded at $y = 0$ and $y = L_y$. The z-axis is directed vertically upward, the height $z = 0$ is defined as the height of the still water level [*Garnier*, 2006].

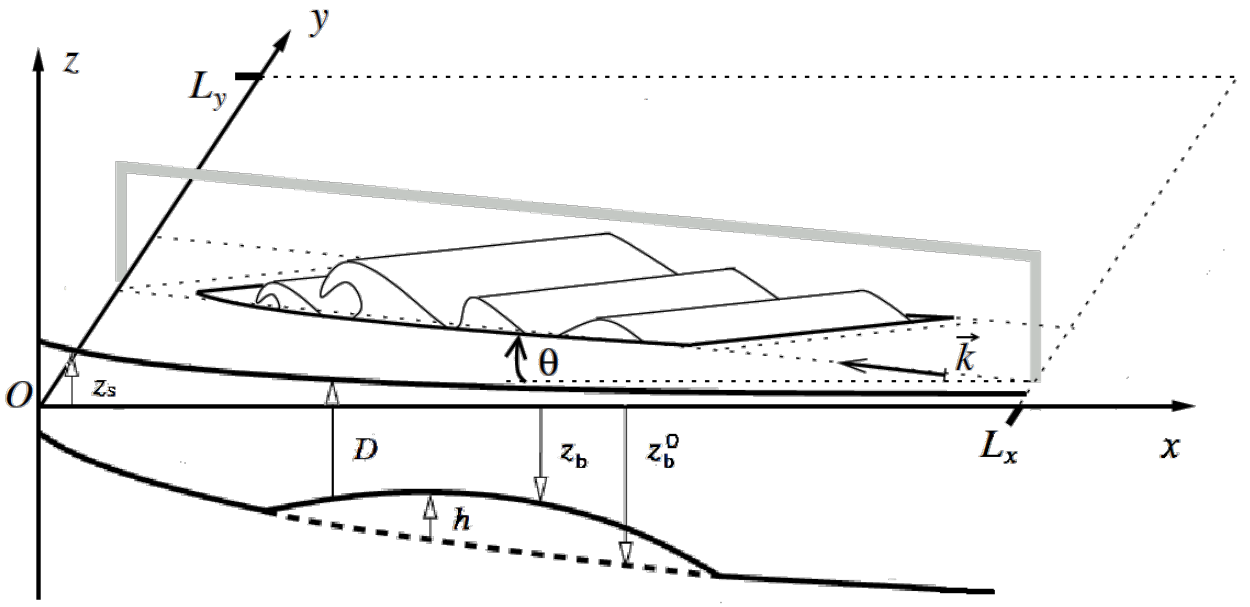

Figure 3: Schematic view of the study area. The vertical direction is represented by z, x and y represent the horizontal in the offshore and longshore direction respectively. The boundaries of the system are located at $x = 0$, $y = 0$, $x = L_x$ and $y = L_y$. The mean depth D is defined as the difference between z_s (the mean sea level) and z_b (the bed level). Furthermore, h is the perturbation of the initial bed level z_b^0: $h = z_b - z_b^0$. Waves propagate in the direction of wave vector $\vec{k}$, with an angle θ with respect to normal wave incidence. Figure modified after *Garnier* [2006].

2.2 Hydrodynamics

2.2.1 Currents

The model solves hydrodynamic equations, which are coupled with sediment equations to finally calculate a new bed pattern that consequently is used as input for the hydrodynamics in the next time step, see also figure 4. The hydrodynamics are governed by two parts. The first contains the currents, satisfying the following equations:

$$\frac{\partial D}{\partial t} + \frac{\partial}{\partial x_j}(D v_j) = 0, \tag{1}$$

$$\frac{\partial v_i}{\partial t} + v_j \frac{\partial v_i}{\partial x_j} = -g\frac{\partial z_s}{\partial x_i} - \frac{1}{\rho D}\frac{\partial}{\partial x_j}(S'_{ij} - S''_{ij}) - \frac{\tau_{bi}}{\rho D}, \tag{2}$$

namely the water mass conservations equation (1) and momentum balance equations (2), together known as the phase averaged nonlinear shallow water equations [*Mei*, 1989]. Herein, the Einstein notation is used, i.e., if an index appears twice in a term, a summation over its values is assumed. In these equations, v_i is the depth- and wave-averaged velocity in direction $i = (x, y)$, D the mean depth, defined as $z_s - z_b$ (the mean sea level, the bed level respectively), g is the gravity acceleration (9.8 m s^{-2}), ρ the water density of 1024 kg m^{-3} and p the bed porosity, set to 0.4. Furthermore S' and S'' are stress tensors, named the wave radiation and the Reynolds stress tensors, which describe transfer of momentum by waves and turbulent eddies, respectively. The bed stress is represented by τ_{bi}, the components of the bed stress vector. Through wave radiation stress S' and bed stress τ_b, the influence of waves on currents is taken into account.

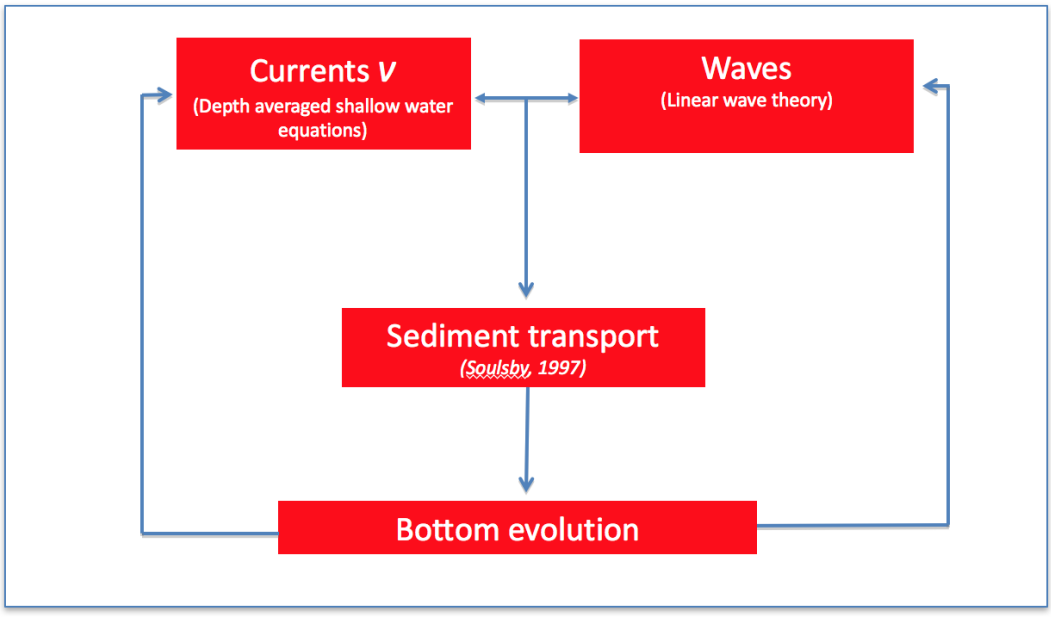

Figure 4: Schematic model overview of Morfo55.

2.2.2 Waves

The second part of the hydrodynamics contains the waves. One of the governing equations is the wave energy balance:

$$\frac{\partial E}{\partial t} + \frac{\partial}{\partial x_j}((v_j + c_{gj}E)) + S'_{ij}\frac{\partial v_j}{\partial x_i} = -\epsilon. \tag{3}$$

Here, $E = \rho g H_{rms}^2/8$ is the wave energy density with $H_{rms}(x, y, t)$ the root-mean-square wave height. Furthermore, ϵ is the wave energy density dissipation due to breaking ϵ_{br} [*Thornton and Guza*, 1983] and bottom friction ϵ_{fr} [*Horikawa*, 1988]. The group velocity c_{gi} can be related to k, the wave number, by using the dispersion relation from linear wave theory:

$$\sigma_\omega^2 = gk \tanh kD, \tag{4}$$

where σ_ω is the intrinsic frequency (the frequency measured in a frame with the current velocity v_i). The absolute frequency ω is equal to $\sigma_\omega + v_j k_j$, where k_i denotes the components of the wave vector with $i = (x, y)$ [*Mei*, 1989]. Moreover, ω is held constant. Together with the law of refraction

$$\frac{\partial k_x}{\partial y} = \frac{\partial k_y}{\partial x}, \tag{5}$$

k_i is determined. The waves are influenced by the currents through current refraction and depth D.

2.3 Sediment transport and bottom evolution

Regarding morphodynamics, the bed evolution equation,

$$\frac{\partial z_b}{\partial t} + \frac{1}{1-p}\frac{\partial q_j}{\partial x_j} = 0, \tag{6}$$

is used, which follows from the conservation of sediment mass. In equation (6) the total load sediment transport components are denoted as q_i and can be calculated in several ways. Here the Soulsby-Van Rijn formulation from *Soulsby* [1997] is chosen, so that

$$q_i = \alpha(v_i - \gamma u_b \frac{\partial h}{\partial x_i}), \tag{7}$$

with α the stirring factor, γ the bed slope coefficient and u_b the root-mean-square wave orbital velocity amplitude at the bottom. Both α and u_b are parametrised according to *Soulsby* [1997]. In equation (7), γ is the bedslope parameter. The perturbation $h(x, y, t)$ from the original bed level z_b^0, is defined as $z_b - z_b^0$.

2.4 Boundary conditions

The following boundary conditions are imposed. At the lateral boundaries of the domain, $y = 0$ and $y = L_y$, the variables D, u, v, H_{rms}, z_b and its y-derivatives were imposed to be the same (periodic boundary conditions). At the shore boundary, both velocity components and the sediment transport component normal to the shore are zero. At the offshore boundary, the velocity components exponentially decay, i.e. $v_i(x, y, t) = v_i(L_x, y, t) \exp \frac{L_x - x}{\kappa_i}$ for $L_x \geq x$, where κ can be seen as a decay parameter. Moreover, at this boundary the root-mean-square of the wave height is imposed, i.e. $H_{rms}(L_x, y, t) = H^0_{rms}$. Likewise, at this boundary the angle of wave incidence is prescribed, i.e. $\theta(L_x, y, t) = \theta^0$. Finally, $\omega = 2\pi/T$ is set to a constant value at this boundary.

2.5 Numerics

With these fully coupled equations and boundary conditions, the dynamical variables $z_s(x, y, t)$, $z_b(x, y, t)$, both horizontal velocity components u and v in the x and y direction respectively, the wave angle $\theta(x, y, t)$ and the wave energy density $E(x, y, t)$ can be calculated. To this end, the scalar- and vector fields are discretised in space and time. In space, a rectangular staggered grid is considered. Scalar variables are defined at the centre of each grid cell. Vector components in the x-direction belonging to a vector at grid point (i, j), are calculated at $(i - \frac{1}{2}, j - 1)$, vector components in the y-direction are calculated at $(i - 1, j - \frac{1}{2})$. Time-integration of these equations is performed by a second order Adams-Bashforth scheme after an initial integration using a forward Euler first order scheme, the spatial derivatives are calculated by finite difference methods, using the central second order approximation. [*Garnier*, 2006; *Garnier et al.*, 2008].

3 Methodology

3.1 Model setup

The model is run for a single barred beach, given by the profile of *Yu and Slinn* [2003], based on the profile of the sandy beach of Duck, California:

$$z_b^0(x) = -a_0 - a_1(1 - \frac{\beta_2}{\beta_1}) \tanh [\frac{\beta_1 x}{a_1}] - \beta_2 x + a_2 \exp [-5(\frac{x - x_c}{x_c})^2], \tag{8}$$

with the specific parameter values the same as in *Garnier et al.* [2008, 2010], in order to make the results comparable: a_0, the depth at the shore boundary is set to 0.25 m, $a_1 =$ 2.97 m, β_1, the shore slope coefficient close to the shore, has a value of 0.075 and $\beta_2 = 0.0064$ the offshore slope coefficient. Furthermore, the longshore bar is located at $x_c = 80$ m, with an amplitude of $a_2 = 1.5$ m. This profile is morphologically steady.

symbol	**description**	**value**
Hydrodynamics		
Currents:		
ρ	water density	1024 kg m^{-3}
κ	velocity decay parameter	3
L_x	offshore domain length	250 m
L_y	longshore domain length	2000 m
Waves:		
H_{rms}^0	imposed wave height at $x = L_x$	1 m
T	imposed wave period	6 s
θ^0	imposed angle of wave incidence at $x = L_x$	variable
γ_b	wave breaker index	0.6
c_d	bottom friction coefficient	0.01
Sediment		
$h(t = 0)$	initial perturbation	0.02 m
z_0	roughness length	0.06 m
d_{50}	sediment size	0.00025 m
p	bed porosity	0.4
s	relative sediment density	2.65
γ	bedslope parameter	5
Numerics		
Δy	grid size in longshore direction	10 m
Δx	grid size in offshore direction	5 m
Δt	time step	0.05 s
Moac	morphological acceleration factor	90

Table 1: List of model parameters.

Therefore, at the start of a model run, a random initial bottom perturbation with an amplitude 0.02 m has been imposed over the entire domain in order to trigger growth of sandbars. The domain is defined as $0 \leq x \leq L_x = 250$ m and $0 \leq y \leq L_y = 2000$ m, divided by grid cells of $(\Delta x, \Delta y) = (5,10)$ m. The time step is set to $\Delta t = 0.05$ s, the morphodynamics are accelerated with a factor 90. Every model run, a total of $6{\times}10^6$ time steps has been executed, which equals 312.5 days of real time evolution. Furthermore, bedslope parameter γ is given the value of 5 and wave breaker index γ_b that appears in the formulation of ϵ_{br} [*Thornton and Guza*, 1983], has been set to 0.6. The roughness length, a parameter in the parametrisation of α [*Soulsby*, 1997], is chosen to be 0.06 m, all as in *Garnier* [2006]. For all experiments, $H^0_{rms} = 1$ m with a period T of 6 s.
An overview of all model parameters can be found in table 1.

3.2 Experiments

In order to finally be able to obtain the main objective, the following experiments have been conducted of which the names can be found in table 2.

First of all, the basic state is analysed, i.e., the state at which the bottom evolution has been turned off. This has been done for several constant angles of wave incidence, namely for normal wave incidence $\theta^0 = 0°$ and oblique incidence, $\theta^0 = 4°, 10°$. This experiment is denoted as 'case0'. From this experiment, it is possible to check the behaviour of the hydrodynamics.

In the reference case or 'case1', $\theta^0 = 0°$ (constant normal wave incidence) and bottom evolutions are allowed. Together with 'case2' in which constant oblique wave angles are imposed, model results can be compared to results of *Garnier et al.* [2008] to verify the model setup. Specifically, in 'case2i' , θ^0 has been set to values of -2°, +1°, 2°, 3°, 4°, 5°, 6°, 7° and 8°, starting with small perturbations from the initial bed level.

Also in experiment 'case2m', the angle of wave incidence is held constant in time. The runs begin with sandbars that were formed for $\theta^0 = 0°$. Constant oblique angles of wave incidence of θ^0 = -2°, +2°, 4°, 6° and 8° are imposed. The main focus for this case is the time for which the formed mature sandbars at $\theta^0 = 0°$ adapt to the new angle of wave incidence.

This time will subsequently be used to estimate the period of the imposed periodically varying wave angles in case3:

$$\theta^0 = \theta^0_{max} \sin(\omega_{var} t) + \theta^0_0, \tag{9}$$

where θ^0_{max} denotes the amplitude of the variation, θ^0_0 the average of the wave incidence and $\omega_{var} = 2\pi/T_{var}$ the angular frequency, with T_{var} the period of the variation. In experiment 'case3Tj' several runs will be done for $T_{var} = 7$ days, 28 days, 56 days, 112 days and 224 days with $\theta^0_{max} = 2°$. In experiment 'case3Aj', T_{var} will be held constant to 28 days with amplitudes θ^0_{max} of 0.5°, 1°, 2°,4°,6° and 8°. Here 'j' denotes the mean angle of incidence: $j = 0, 2$ and 4, resembling $\theta^0_0 = 0°$, 2° and 4°. The analysis of this case will directly form the answer to the objective of this study and therefore answer the main question.

name of run	description
case0	basic state: hydrodynamical model run for $\theta^0 = 0°$, 4° and 10°.
case1	reference case: constant normal wave incidence from initial perturbation
case2i	constant oblique incidence from initial perturbation, θ^0 = -2°, +1°, 2°, 3°, 4°, 5°, 6°, 7°, 8°.
case2m	constant oblique incidence from mature bars, θ^0 = -2°, +2°, 4°, 6°, 8°.
case3Tj	periodically changing wave incidence from initial perturbation. for $\theta_0^0 = 0°$, 2°, 4°(denoted with $j = 0, 2, 4$ respectively), forcing periods T_{var} = 7, 28, 56, 112, 224 days are imposed, all with an amplitude $\theta^0_{max} = 2°$.
case3Aj	periodically changing wave incidence form initial perturbation. for $\theta_0^0 = 0°$, 2°, 4°(denoted with $j = 0, 2, 4$ respectively), forcing amplitudes , θ^0_{max} = 0.5°, 1°, 2°,4°,6°, 8° are imposed, all for a period of T_{var} = 28 days.

Table 2: List of model run names. Here θ^0 is the imposed angle of wave incidence, T_{var} the period of the imposed angle of wave incidence in case of periodically changing θ^0 with amplitude θ^0_{max}. The mean angle of wave incidence is denoted as θ^0_0 in these cases.

3.3 Global analysis

In order to analyse the results of the experiments described in section 3.1, global analysis of bottom perturbation h is used, following *Garnier* [2006]:

$$||h|| = (\overline{h^2})^{1/2}. \tag{10}$$

This is the root-mean-square height of the bottom perturbation or mean deviation from the initial bed level, $\frac{1}{2}||h||^2$ is consequently defined as the potential energy density as in *Vis-Star et al.* [2008]; *Garnier et al.* [2010]; *Castelle and Ruessink* [2011]. In equation 10, $\overline{h^2}$ is the domain wide averaged square of h, calculated as

$$\overline{h^2} = \frac{1}{L_x L_y} \int_0^{L_x} \int_0^{L_y} h^2 \, dxdy. \tag{11}$$

It is also convenient to define

$$\sigma = \frac{1}{||h||^2} \frac{d}{dt} (\frac{1}{2}||h||^2), \tag{12}$$

which represents the global growth rate of the bottom perturbations.

3.4 Fourier transformation

To analyse the typical spacing of the sandbars, further analysis of h is applied. For each time t an alongshore transect of h at $x = 50$ m is taken, analysed by means of a discrete Fourier transform:

$$H(k_l) = \sum_{j=1}^{N_y} h(50, y_j) \exp(-i \frac{2\pi}{N_y}(j-1)(l-1)). \tag{13}$$

In this expression, $H(k_l)$ is the Fourier coefficient corresponding to wave number $k_l = \frac{2\pi(l-1)}{L_y}$, $N_y = L_y/\Delta y$ and $y_j = j\Delta y$, where $j, l = 1, 2, 3, ..., N_y$. The absolute value of $H(k_l)$, $|H(k_l)|$, is interpreted as the height of the sandbars corresponding to k_l. The wave number k_l corresponds with wave length λ_l by $\lambda_l = 2\pi/k_l$, where $\lambda_l = L_y/(l-1)$, the wave length of mode l [*Garnier*, 2006].

4 Results

4.1 Basic state properties

The basic state is defined as the state of the system without any initial perturbation. This state is morphologically steady, i.e., no bed level deviations occur. Furthermore, this state gives insight in currents and wave behaviour of the model and is longshore uniform. In figure 5, the behaviour of hydrodynamic quantities in the offshore direction are shown after the model has been spun up for angle of wave incidence of $\theta^0 = 0°$ (blue), $\theta^0 = 4°$ (orange) and $\theta^0 = 10°$ (green). The figure for z_b clearly denotes the existence of the longshore bar at $x = 80$ m. At this bar, waves decrease in height (see H_{rms}), since their wave energy is lost due to breaking and friction revealed by a local maximum of $\epsilon = \epsilon_{br} + \epsilon_{fr}$, the wave energy dissipation rate. Besides, the water level rises at the longshore bar and near the coast, as z_s denotes. For normal wave incidence, the wave direction θ is not influenced by the existence of the longshore bar, however, refraction is noticed for 4° and 10°. Moreover, for these non zero wave angles, a longshore current v is observed, highest values of 0.3 m s^{-1} for $\theta^0 = 10°$ at the longshore bar and near the coast, where the wave height decreases to 0 m.

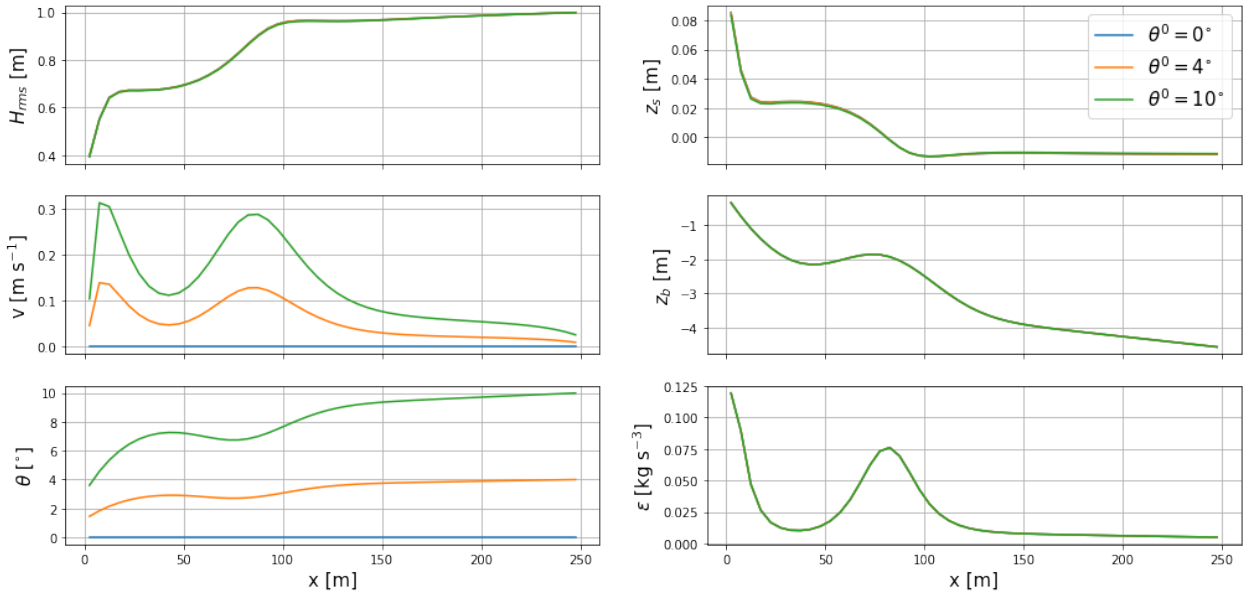

Figure 5: Dependence of basic state variables on cross-shore distance x of a single barred beach with a longshore bar at $x = 80$ m. Here, no bed level deviations are taken into account. In the left column, from top to down: H_{rms}, the significant wave height, v, the current in the $y-$direction, and θ, the wave angle. At the right hand side: z_s, the mean sea level, z_b, the bed level and ϵ, the wave energy dissipation due to wave breaking and friction near the bottom. Wave refraction (declining θ) and dissipation (declining H_{rms}) at the longshore bar are clearly observed.

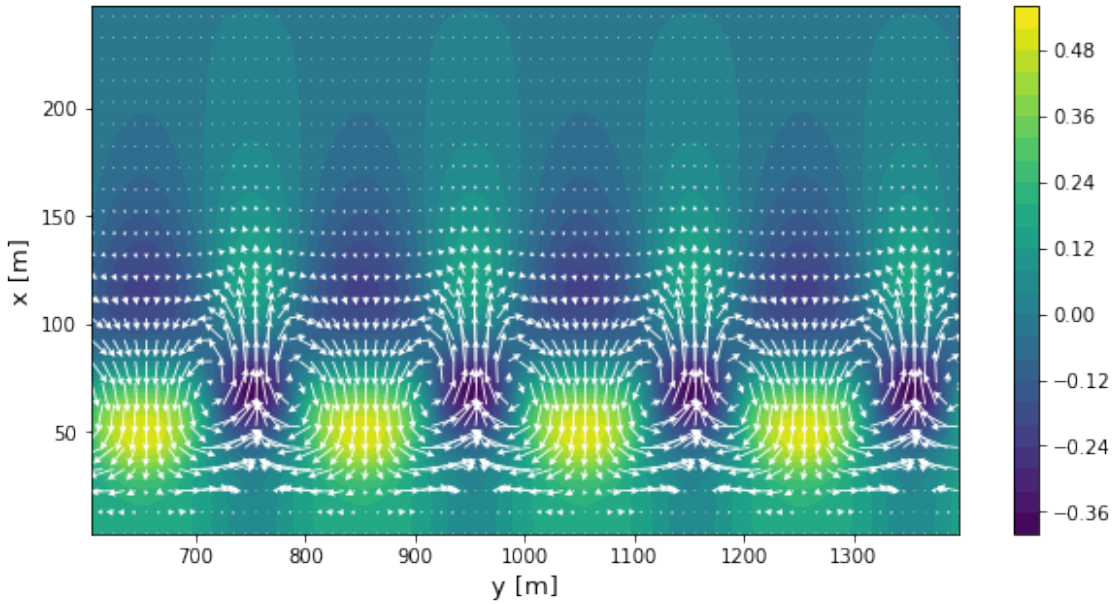

Figure 6: Pattern of bed level deviations h [m] in filled contours with on top, shown as the white arrows, the currents for the equilibrium situation of the reference case at $t = 312.5$ days. After 80 days of modelled time, these patterns were observed to be constant for the rest of the model run. Strongest offshore currents are observed for the most negative values of h (rips), which is characteristic for rip current systems.

4.2 Reference case: normal incidence

In case of normal wave incidence with allowed bed level deviations h, h (the filled contours) is shown in figure 6 after 312.5 days of modelled time together with characteristic currents (white arrows). The biggest offshore currents are observed at locations for most negative values of h, i.e., rips, while onshore currents are mostly present for the most positive values of h (shoals). In figure 7, the evolution of $||h||$, the mean deviation from the initial bed level, in time is shown. As $||h||$ starts to increase, the global growth rate σ is positive and forms a maximum in time, which is called the linear regime as in *Garnier et al.* [2010]. Hereafter, nonlinear effects cause a reduction of the growth rate, and saturation of the sandbars takes place: $||h||$ grows until a new dynamical equilibrium is reached: the saturated state. In terms of σ, the state is called saturated when $\sigma(t) \simeq 0$ for the first time after the linear regime. When $\sigma = 0$ for all times, the state is denoted as the equilibrium state. The time t_i is the time at which the saturated state is reached and is equal to 21 days for constant normal wave incidence, the equilibrium situation is reached after 80 days of modelled time.

The wave length of the dominant mode, which is the mode for which $|H(k_l)|$ has a maximum, is denoted by $l = m$. Explicitly to mention is λ_m, the dominant wave length or the dominant longshore spacing between shoals. In the saturated state, the bars reach their dominant spacing λ_m of 200 m, but still are not in a steady equilibrium: $||h||$ still varies (figure 7). Moreover, sandbars still have not been adapted to a final shape, the entire system has still

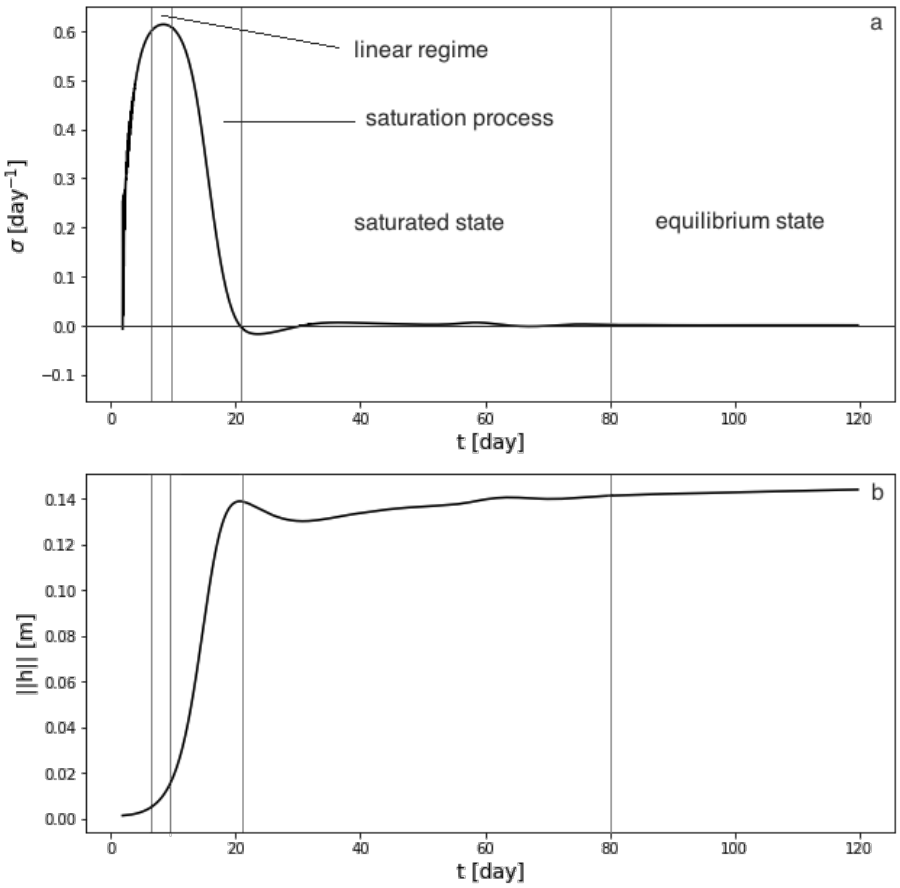

Figure 7: Results for constant normal wave incidence, the reference case. (a) Global growth rate σ of the bottom perturbations versus time. The maximum of σ denotes the linear regime of the system. The saturation process is the process in which the growth decreases. The first time σ becomes 0 after initial growth, the system reaches its saturated state. For $\sigma(t) = 0$ constant in time, the system is in equilibrium [*Garnier et al.*, 2010]. (b) Time series of $||h||$, the mean deviation from the initial bed level.

dynamical features. To visualise this, $h(x = 50\text{ m}, y, t)$ is shown in figure 8. After $t \approx 20$ days, bars arise at $x = 50$ m for every y. A total of 11 bars has been formed then, but their height varies slightly in time which can be seen from the occasional more yellow parts for individual rips in time. Around $t = 50$ days, $y = 1000$ m, it appears that two rips form a single new rip for the shoal in between has been vanished. After the system is adapted to this new situation of 10 bars within the domain, $h(x = 50\text{ m}, y, t)$ keeps more or less constant in time: the equilibrium state. Up to small differences due the use of a slightly different initial perturbation, these results are similar to the results of *Garnier et al.* [2008].

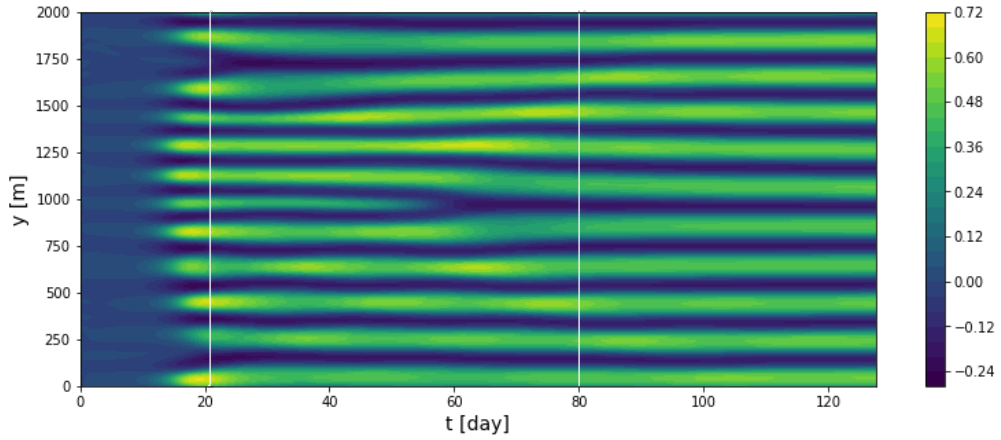

Figure 8: Filled contour plot for $h(x = 50 \text{ m}, y, t)$ [m] for constant normal wave incidence, the reference case. At every t, a transect at $x = 50$ m is taken for h. Marked are the beginning of the saturated state (left white line) and the equilibrium state (right white line), as in figure 7. Within the saturated state, two rip channels merge and the shoal in between vanishes. In the equilibrium state, no changes occur.

4.3 Case 2: constant forcing with oblique incidence

4.3.1 Case2i: from initial perturbation

Time series of $||h||$, the mean deviation from the initial bed level, for different offshore angles of wave incidence θ^0 are shown in figure 9a. In particular, results for $\theta^0 = 2°$, $4°$, $6°$ and $8°$ are shown and will be discussed in detail. The more oblique the wave incidence, the longer it takes to reach the saturated state. For $2°$ (green line, black is the reference case), it is reached after 24 days and for $4°$ (blue) after 39 days. For $\theta^0 = 6°$ (red), σ does not reach zero after the growth has started within the modelled time, for $8°$(orange) no bar development is observed at all. The bars that do develop, migrate along the shore with a speed that increases with increasing θ^0: $c = 11$ m day^{-1} for $2°$, $c \approx 20$ m day^{-1} for $4°$ and $c \approx 33$ m day^{-1} for $6°$ at the end of the model run. The dominant spacing λ_m increases with increasing θ^0 with $\lambda_m = 200$ m, $\lambda_m = 250$ m and $\lambda_m \approx 285$ m for $\theta^0 = 2°, 4°, 6°$ respectively. In contrast to normal wave incidence, for oblique incidence, the equilibrium state is never reached. As can be seen for $4°$ in figure 9b, (but this also holds for $2°$), during the entire model run, the bars widen and narrow. Even after 300 days of modelled time, at $y \approx 1000$ m, a bar vanishes and two rips merge. In general, the shoals are skewed in the direction of the current and are narrower in the y-direction compared to the reference case.

Interestingly, $||h||$ is bigger for $2°$ than for $0°$ whereas $||h||$ is smaller for $4°$. Using all experiments, the dependence of $||h||$ with respect to θ^0 is plotted in figure 10 (solid black line): $||h||$ has a maximum for $\theta^0 = 3°$, which is in agreement with *Garnier et al.* [2008].

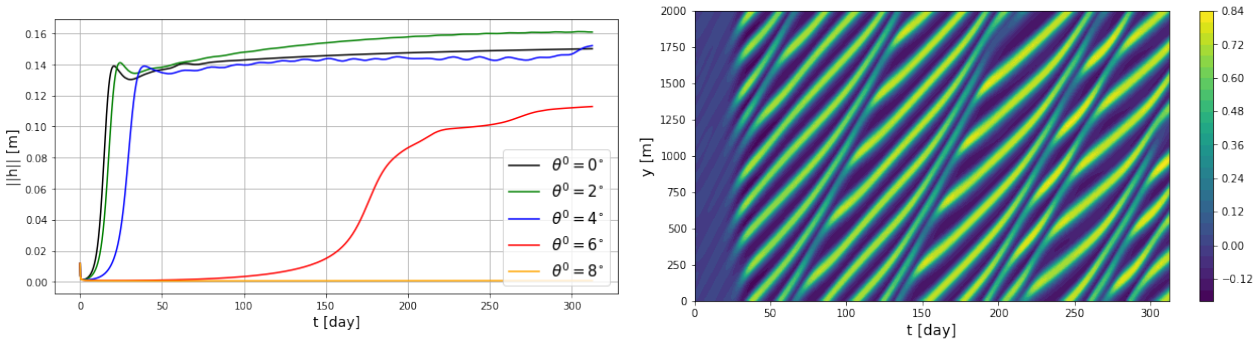

(a) (b)

Figure 9: Results for case2i, constant forcing with oblique angle of wave incidence θ^0. (a) Evolution in time of $||h||$, the mean deviation from the initial bed level. Black denotes the reference case (θ^0= 0°). In green: $\theta^0 = 2°$, blue: $\theta^0 = 4°$, red: $\theta^0 = 6°$ and in orange $\theta^0 = 8°$. For $\theta^0 = 6°$ it takes much longer to reached a saturated state, for $\theta^0 = 8°$ no sandbars are observed at all. (b) Filled contour plot for $h(x = 50\text{ m}, y, t)$ [m] for $\theta^0 = 4°$. Bars migrate alongshore and change in form through time.

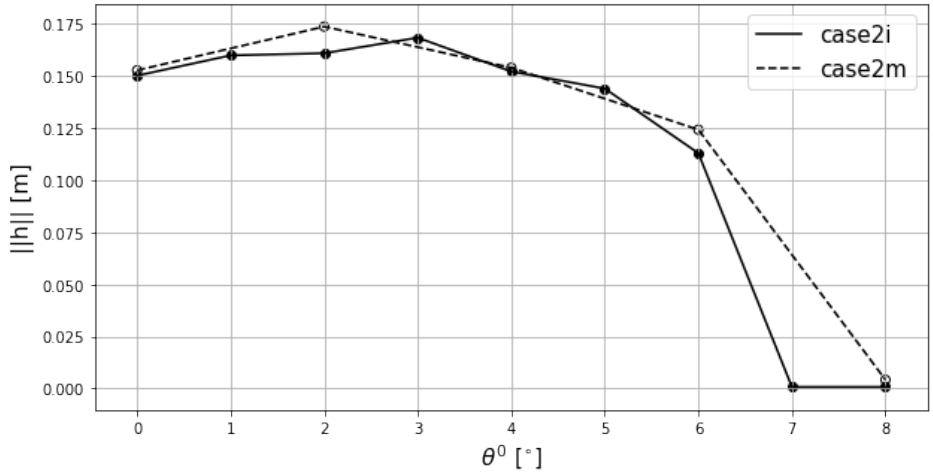

Figure 10: Dependence of $||h||$ for different values of constant angle of wave incidence θ^0 for case2i (growth from initial perturbation, solid black) and case2m (growth from existing bar patterns, dashed black). As in *Garnier et al.* [2008], the maximum of $||h||$ is observed at $\theta^0 = 3°$ in case2i.

4.3.2 Case2m: from mature sandbars

Figure 11a shows time series of $||h||$ for different θ^0. In each case, the initial state is a pattern of mature sandbars that resulted from normal wave incidence. For every non zero θ^0, directly after the change the bars decrease compared to the reference case (dashed black line). For 2°(green), growth of $||h||$ takes over within 3 days and eventually $||h||$ becomes higher than the reference case. This is also the case for 4°(blue). For 6°(red) it takes much longer for the growth to overtake the initial decrease of $||h||$, for 8°(orange) no growth is observed at

all. The mean heights $||h||$ of the sandbars in equilibrium are shown in figure 10 (dashed line). Since this behaviour directly after the start of the model run in $||h||$ and so in σ, is different than for a model run from initial perturbation, the typical time scale t_i cannot be used. In order to provide insight in the time it takes the system to adapt to a new angle of wave incidence, an adjustment time t_a is used instead and is defined as the time at which σ has a minimum after its global maximum.

For $\theta^0 = 2°$, t_a is equal to 15 days, for $4°$, $t_a = 26$ days, $t_a = 73$ days for $6°$ and for $8°$, no adjustment time is found since only decay is observed. For $2°$ and $4°$, the bars keep steady in time for the entire model run (figure 11b). The bars migrate longshore with $c = 9$ m day^{-1}, 23 m day^{-1} for $2°$ and $4°$ respectively and 32 m day^{-1} for $\theta^0 = 6°$, so both t_a and c increase with increasing θ^0. Regarding the preferred wavelength λ_m, it turns out that $\lambda = 200$ m for both $\theta^0 = 2°$ and $\theta^0 = 4°$. For $\theta^0 = 6°$, $\lambda \approx 285$ m as it was for $6°$ from initial perturbation.

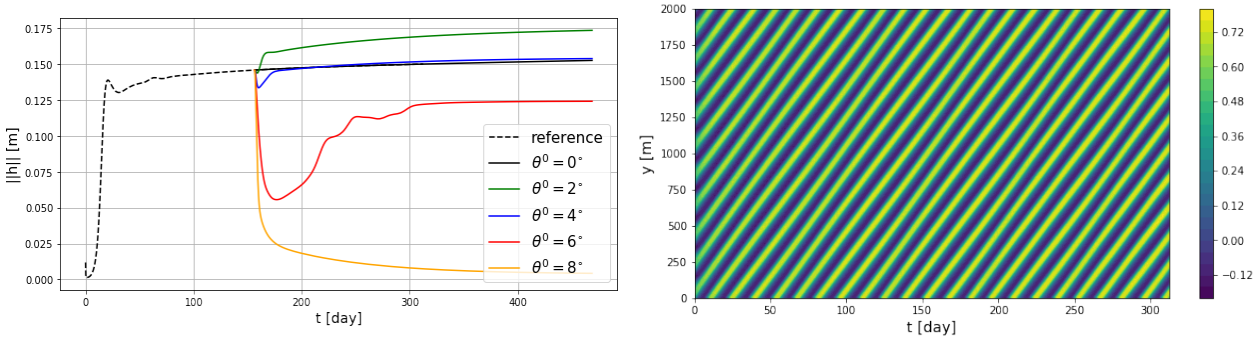

(a) (b)

Figure 11: Results for case2m. For the first 150 days, constant normal forcing was used and sandbar patterns formed. After that, a constant oblique angle of wave incidence θ^0 was imposed. (a) Time evolution of $||h||$. The dashed black line denotes the reference case for the first 150 days. The different constant angles of wave incidence which were imposed after 150 days are denoted by the solid lines with in green: change to $\theta^0 = 2°$, blue: $\theta^0 = 4°$, red: $\theta^0 = 6°$ and in orange $\theta^0 = 8°$. For $\theta^0 = 8°$, existing bars break fully down. (b) Filled contour plot for $h(x = 50 \text{ m}, y, t)$ [m] after the change of wave angle to $4°$. Bars migrate alongshore but remain their shape in time.

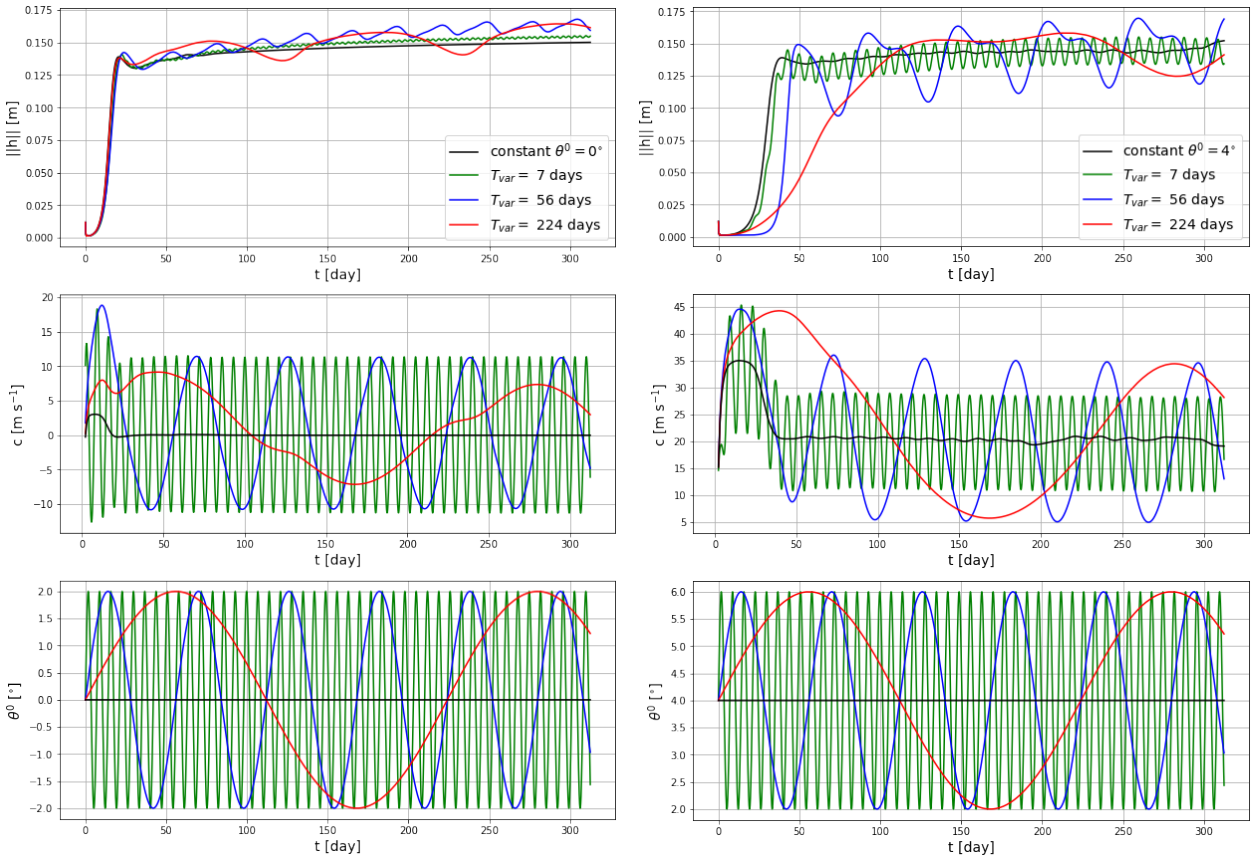

(a) $\theta_0^0 = 0°$, $\theta_{max}^0 = 2°$

(b) $\theta_0^0 = 4°$, $\theta_{max}^0 = 2°$

Figure 12: Results for case3T, periodic forcing with several periods T_{var}. Upper images show the time evolution of $||h||$. Middle images show the time evolution of the longshore migration c. Lowest images show the imposed angle of wave incidence θ^0 at the offshore boundary. In green: $T_{var} = 7$ days, blue: $T_{var} = 56$ days and $T_{var} = 224$ days (red). Amplitudes of the variation $\theta_{max}^0 = 2°$ with in case of (a): a mean wave direction of 0 ° (black) and (b) a mean of 4° (black). Specific behaviour of $||h||$ depends on T_{var} and θ_0^0.

4.4 Case 3: time dependent periodic forcing

4.4.1 Case3T: varying the forcing period

For case3T, a sinusoidally varying angle of wave incidence θ^0 was imposed. This was done with an amplitude of the variation of $\theta_{max}^0 = 2°$, for on average normal incidence ($\theta_0^0 = 0°$; case3T0), for $\theta_0^0 = 2°$(case3T2), and for $\theta_0^0 = 4°$(case3T4). For every case, several periods of the variation were imposed: $T_{var} = 7$ days, 28 days, 56 days, 112 days and 224 days. For case3T0 and case3T4, typical results of the time evolution of $||h||$, the mean deviation from the initial bed level and time evolution of the longshore migration c, for short (T_{var}= 7 days, green), middle (T_{var}= 56 days, blue) and long (T_{var}= 224 days, red) periods are shown in figure 12. The solid black line denotes the constant forcing corresponding to the mean of the periodic forcing.

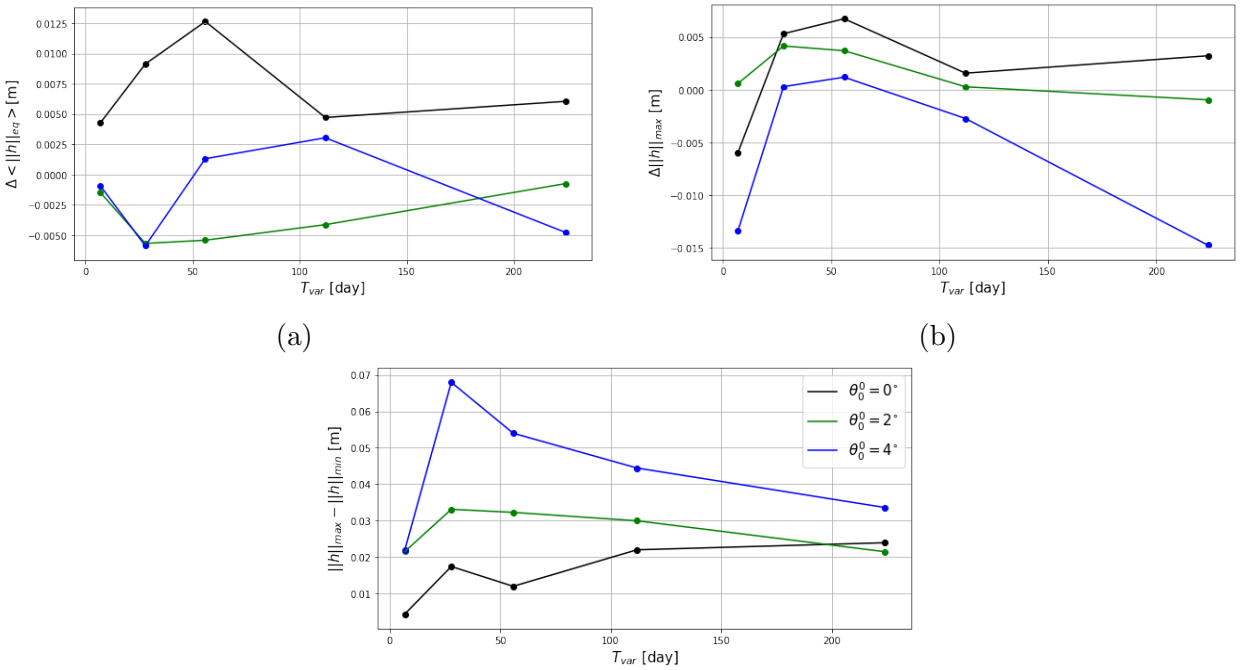

Figure 13: Analysis of the properties of $||h||$ after initial growth as function of forcing period T_{var} based on experiments with different mean values of variation in angle of wave incidence θ_0^0 (case3T). In black, $\theta_0^0 = 0°$, green: $\theta_0^0 = 2°$ and blue: $\theta_0^0 = 4°$. (a) The difference between the average value of $||h||$ as result of time varying forcing and the average value of $||h||$ from constant wave forcing (case2i) is shown as function of T_{var}. (b) For several T_{var}, the difference between the maximum observed value of $||h||$ in case3T and the maximum expected value of $||h||$ based on case2i is shown. (c) The difference between the highest and lowest observed value of $||h||$ after initial growth for case3T. For different values of θ_0^0, the properties of $||h||$ behave differently.

In case of $\theta_0^0 = 0°$, values of $||h||$ are on average roughly the same as the reference case for which the wave incidence was constantly held normal to the coast. The longshore migration of the bars varies sinusoidally with a maximum of $c = 11$ m day^{-1}, the same value as for constant forcing with $\theta^0 = 2°$. For $T_{var} = 112$ days, 224 days this does not hold: the variation in c is not purely sinusoidally and the amplitude declines with larger T_{var}.

For variations with a non zero mean, so for θ_0^0= 2° (case3T2), 4° (case3T4), c varies ±20 m day^{-1}, ±34 m day^{-1} respectively for all T_{var}, with exception of $T_{var} = 7$ days for θ_0^0= 4°. In that particular case, the variation is relatively small with $c = \pm 28$ m day^{-1} as is shown in figure 12b.

A further look into the behaviour of $||h||$ is given in figure 13. In figure 13a, the difference between the average value of $||h||$ as result of time varying forcing and the average value of $||h||$ from constant wave forcing (case2i) is shown as function of T_{var}. Figure 13b shows the difference between the maximum value of $||h||$ for time varying forcing and the theoretical

maximum value expected based on constant forcing as in figure 10. For example, for wave angles varying with 2° around 4°, it is expected that the maximum value of $||h||$ is the value of $||h||(\theta^0 = 3°)$ from constant forcing, since for this angle of wave incidence, the highest bars were observed. Figure 13c shows the difference between the minimum and the maximum value of $||h||$ after initial growth.
Furthermore, not only the mean, maximum and amplitude are analysed, also the phase of the oscillation in $||h||$ with respect to the forcing oscillation is analysed: in figure 14, the response of $||h||$ with respect to angle of wave incidence θ^0 is shown with time t as parameter for the case with zero mean. For figures of the other cases with non zero means, see figure 19 and figure 20 in appendix A.

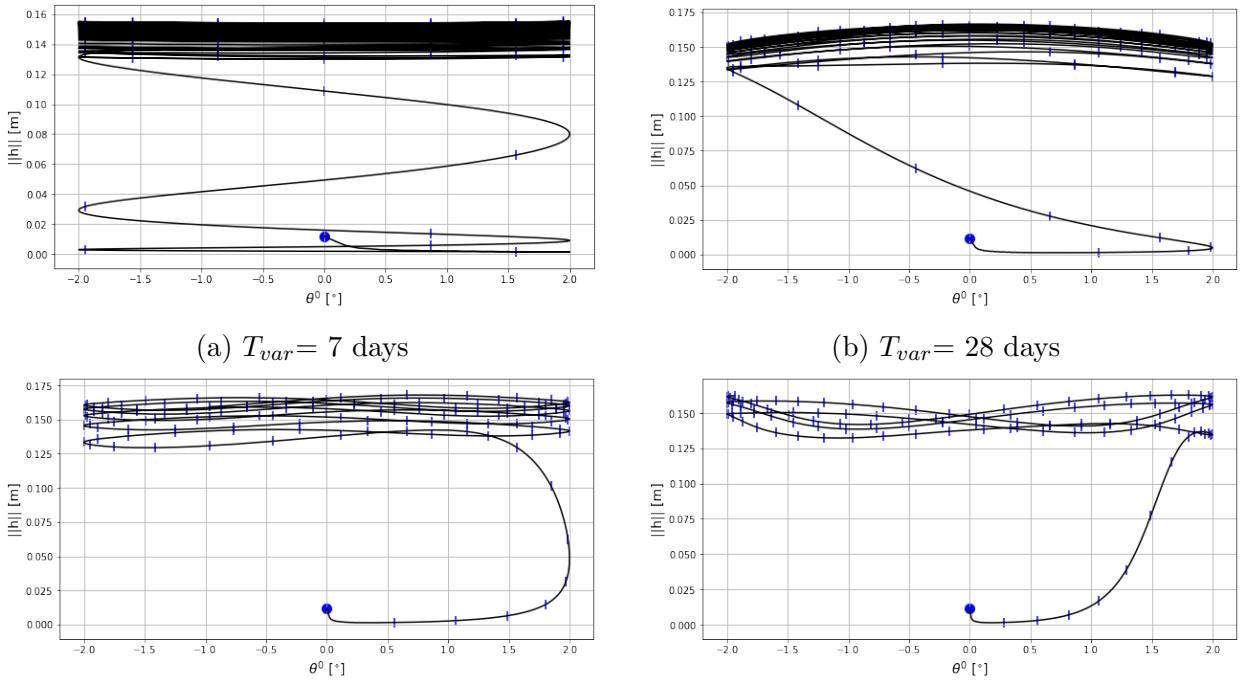

(a) T_{var}= 7 days

(b) T_{var}= 28 days

(c) T_{var}= 56 days

(d) T_{var}= 112 days

Figure 14: Response of $||h||$ with respect to the forcing with angle of wave incidence θ^0 with time t as parameter for the case with zero mean (θ^0_0= 0°, amplitude θ^0_{max}= 2°) and different forcing periods: T_{var} = 7 days, 28 days, 56 days and 112 days. The blue dashes denote a time interval of 2.5 days. Maximum values of $||h||$ are observed at different θ^0 for different T_{var}.

In figure 13 is shown in case of zero mean (black lines; case3T0), that for small T_{var}, $||h||$ is on average slightly larger than the reference case, the maximum value is lower and the amplitude relatively small. From figure 14, the minimum values of $||h||$ are observed at $\theta^0 = 0°$ and the maximum values for $\theta^0 = 2°$, which is the same as expected from constant forcing. For T_{var} = 28 days, 56 days, the mean of the variation is considerably higher than for constant normal forcing, the maximum in $||h||$ is higher than the theoretical maximum and the variation in $||h||$ has a bigger amplitude than for shorter T_{var}. The maximum of $||h||$ is ap-

proximately observed at $\theta^0 = 0°$ instead of at 2° as one would expect from constant forcing. For longer periods, the mean of $||h||$ compared to $T_{var} = 28$ days, 56 days is lower, as is the maximum of $||h||$. However, the amplitudes of $||h||$ are bigger. The maxima are however observed near $\theta^0 = 2°$, as expected.

For case3T2 (green lines), the mean $||h||$ of this variation is slightly lower than $||h||$ for constant $\theta^0 = 2°$ at $T_{var} = 7$ days, 28 days, 56 days. The maximum exceeds the expected maximum in this range. The amplitude of the variation is the biggest for a period of 28 days. In case of $T_{var} = 7$ days, the maximum is around 2°-3°, consistent with constant normal wave incidence, for $T_{var} = 28$ days, 56 days, the maximum is however observed at $\theta^0 = 0.5°, 1.5°$ respectively.
For $T_{var} = 112$ days, 224 days, the mean of the oscillation is higher than for 28 days, 56 days, but the maximum value of $||h||$ and the amplitude are lower. The maximum is observed again between θ^0= 2° and 3°.
In case3T4 (blue lines), these features are approximately the same, however magnified and for $T_{var} = 56$ days, 112 days, the mean of the oscillation in $||h||$ is higher the mean of the constant forcing of 4°. Thereby, the maximum of $||h||$ is observed is at 6° in case of $T_{var} = 7$ days instead of the expected 3°. Also for $T_{var} = 28$ days, the maximum is not located near 3° but near 2°. For T_{var} of 56 days and 112 days, the maximum tends to 3° again.

For the longshore migration c the biggest longshore migrations speeds occur for most oblique angles of wave incidence θ^0, which is expected based on the finding that c scales with θ^0 for constant oblique wave incidences. Plots for c versus θ^0 are shown in figure 21 in appendix A for case3T0. Since this behaviour is equal for non zero mean angles of wave incidence, these cases are not explicitly shown.

4.4.2 Case3A: varying of the amplitude

In case3A, time varying angles of wave incidence were imposed with amplitudes of θ^0_{max} of 0.5°, 1°, 2°, 4°, 6° and 8° for averages of the variation of $\theta^0_0 = 0°$, 2° and 4°. Period of the variation T_{var} is 28 days for all runs. Part of the results are shown in figure 15. The solid black lines denote the constant mean of 0°, 4° respectively. Green denotes $\theta^0_{max} = 1°$, blue $\theta^0_{max} = 4°$, red $\theta^0_{max} = 8°$. The bigger the amplitudes in forcing, the bigger the amplitudes in $||h||$ but not for too big amplitudes, for $\theta^0_{max} = 8°$ on top of $\theta^0_0 = 4°$, no growth is observed at all. The longshore migration speed c scales with θ^0_{max} as well. For zero mean variations in angle of wave incidence, c varies with ±10 m day^{-1} for $\theta^0_{max} = 2°$, ±20 m day^{-1} for $\theta^0_{max} = 4°$ up to ±40 m day^{-1} for $\theta^0_{max} = 8°$. In case of non zero mean, c is observed up to ±53 m day^{-1} in case of $\theta^0_0 = 2°, \theta^0_{max} = 8°$ and ± 56 m day^{-1} for $\theta^0_0 = 4°, \theta^0_{max} = 6°$.

As in figure 13 for case3T, the characteristics of $||h||$ in case3A are further shown in figure 16. Analysis of the response of $||h||$ with respect to the variation in θ^0 is shown in figure 17. For variations with zero mean, for amplitudes $\theta^0_{max} = 0.5°, 1°$, the mean of $||h||$ after the initial growth is similar to constant normal forcing. The maximum is lower than the expected maximum value of $||h||$, the amplitude is relatively small. The maximum value of $||h||$ is found at time the wave forcing angle is normal to the coast.

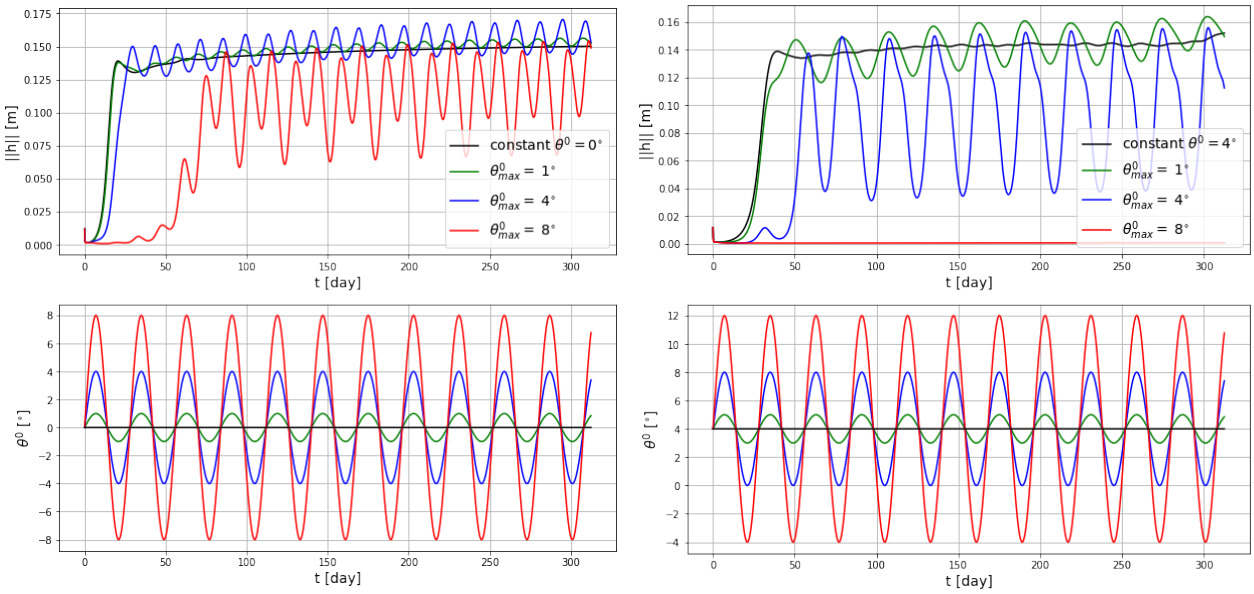

(a) $\theta^0_0 = 0°$, T_{var}= 28 days

(b) $\theta^0_0 = 4°$, T_{var}= 28 days

Figure 15: Results for case3A, periodic forcing with different amplitudes (θ^0_{max}) of the angle of wave incidence for averages of $\theta^0_0 = 0°$(a) and $\theta^0_0 = 4°$ (b). The upper figures are evolution in time of $||h||$, the mean deviation from the initial bed level. The solid black lines denote the constant mean of 0°, 4° respectively. Green denotes $\theta^0_{max} = 1°$, blue $\theta^0_{max} = 4°$, red $\theta^0_{max} = 8°$. The bigger the amplitudes in forcing, the bigger the amplitudes in $||h||$. For $\theta^0_{max} = 8°$ on top of $\theta^0_0 = 4°$ however, no growth is observed at all.

For amplitudes $\theta^0_{max} = 2°, 4°$, the mean is higher and the maximum exceeds the expected value from constant forcing. For an amplitude of 4°, the maximum value is found between 2° and 3° as expected. This is also true for $\theta^0_{max} = 6°$, but at $\theta^0_{max} = 8°$ the maximum is found at $\theta^0 = 5°$. For both amplitudes, the mean is lower than the mean for constant normal wave incidence and also the maximum value of $||h||$ is lower, however the amplitude of the varying response in $||h||$ keeps growing.

In case of variations around a non zero mean, for every amplitude, the mean of the variation in $||h||$ is lower than the constant forcing in the case of a mean of 2°. Only for $\theta^0_0 = 4°$, in the case of $\theta_x = 0.5°, 1°$, the mean is higher than constant forcing. The bigger the amplitude in the wave direction, the lower the mean of $||h||$ is. The maximum keeps below the theoretical maximum is case of a mean wave direction of 2° with amplitudes of 6° and 8° and for a mean of 4° with amplitudes of 4° and 6°.
The response of $||h||$ with respect to the variation in θ^0 as figure 17 for non zero means, is shown in figure 22 and figure 23 in appendix A. For amplitude changing around $\theta^0_0 = 2°$, for amplitudes of $\theta^0_{max} = 0.5°, 1°, 2°$, the maximum of $||h||$ is around 1° and for an amplitude of 4°, around −1°. Expected however are maximum values at $\theta^0 = 3°$ based on results for constant wave forcing. Also for larger amplitudes differences from what is expected are observed, e.g. $\theta^0_{max} = 6°$, the maximum is around $\theta^0 = 2°$. Most remarkable is the case for $\theta^0_{max} = 8°$, in which the maximum of $||h||$ is located at $\theta^0 = 7°$. For the constant forcing

case, not any value of $||h||$ was found at 7°. The same is true for case4A4, where for variation of 6° was found at $\theta^0 = 7°$. For bigger variations, no value of $||h||$ was found, which is in agreement with the constant forcing case. For the other variations, all maximum values of $||h||$ were found at lowest values of θ^0.

For the response of longshore migration c with respect to θ^0, no other behaviour is found than for experiment case3T. To summarise all results, whether the period of the varying angle of wave incidence or the amplitude is changed, the resulting response of $||h||$ is different than expected based on the results of the constant forcing cases, either in height of the sandbars or in corresponding wave direction at which the highest bars arise.

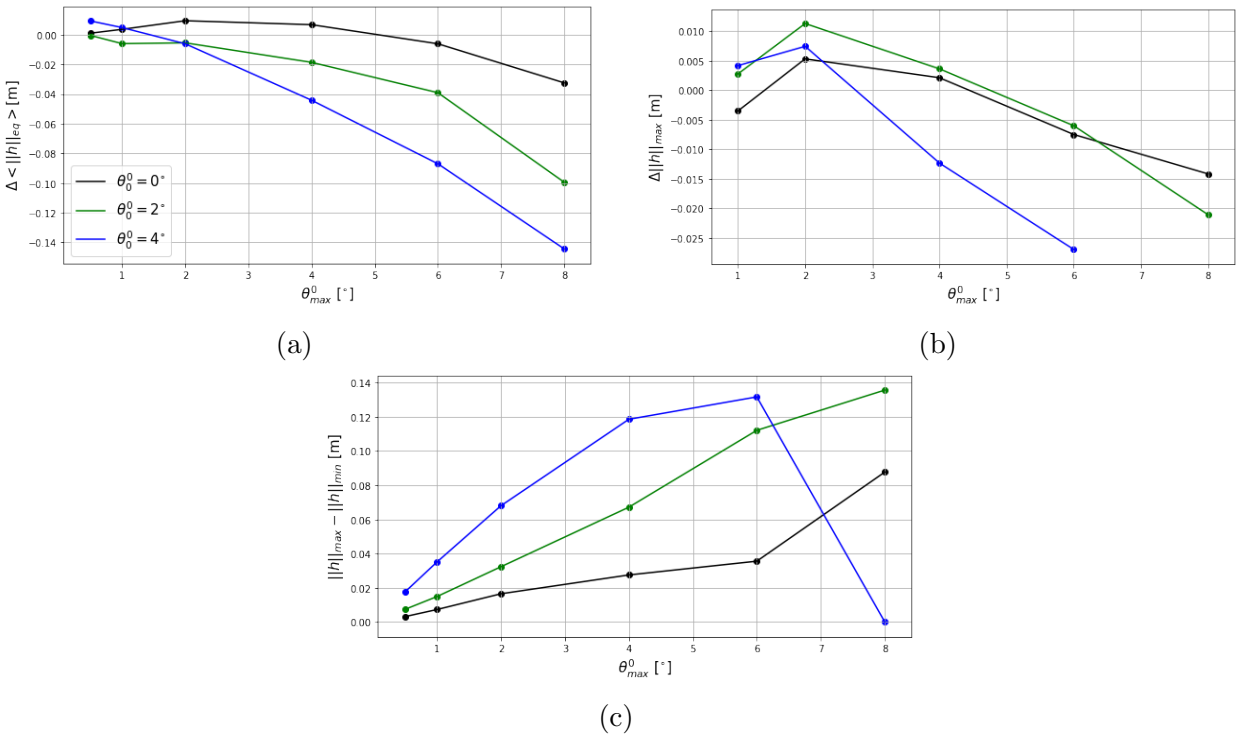

Figure 16: Features of $||h||$ resulting from case3A in which different amplitudes of varying angles of wave incidence θ^0 are investigated, with a period of T_{var}= 28 days and mean values of θ^0 of 0°, 2° and 4°. The same features of $||h||$ as in figure 13 are shown, however, now the different features of $||h||$ are shown as functions of the amplitude. Again, for different θ^0, different behaviour of the features of $||h||$ is observed.

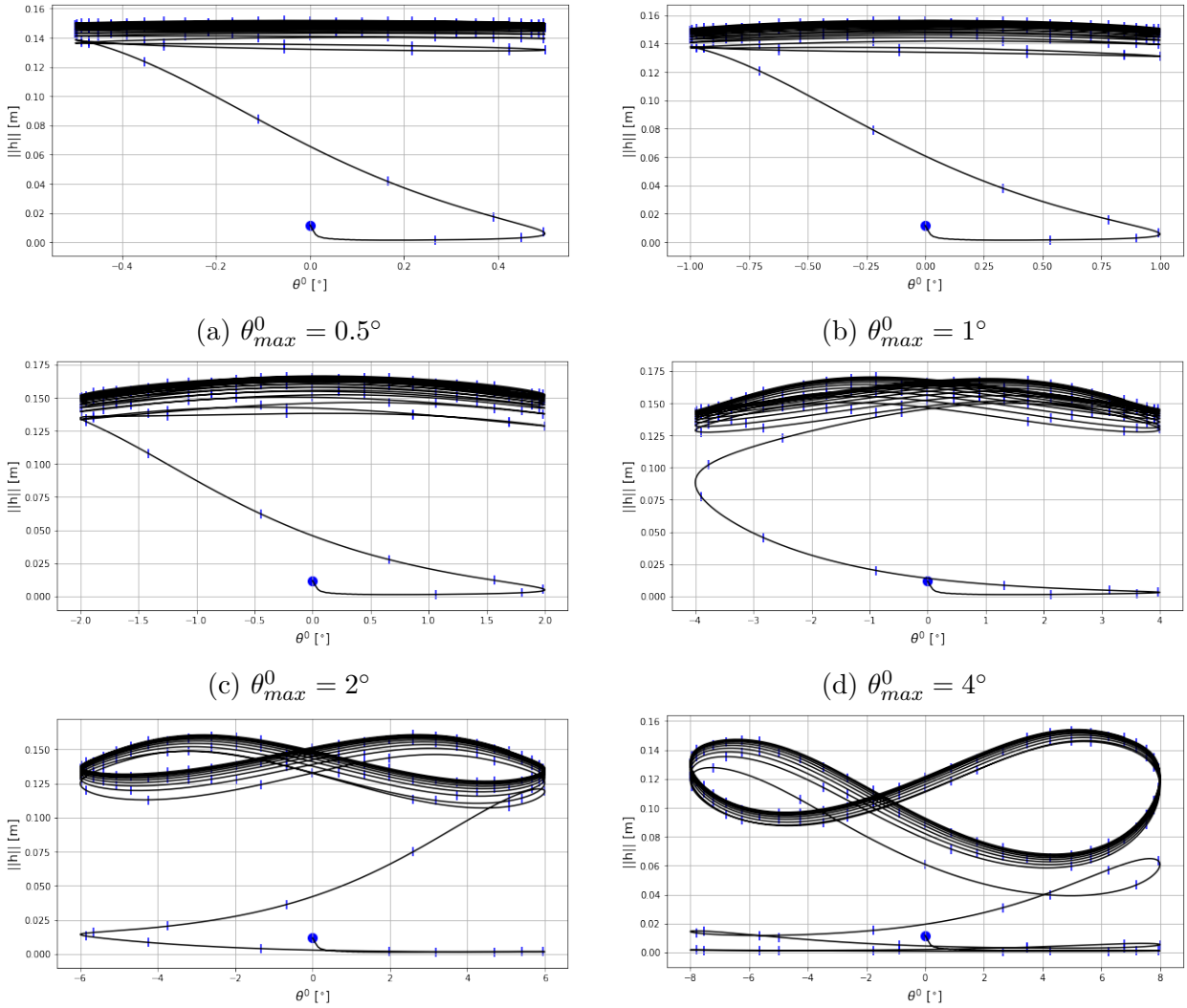

(a) $\theta^0_{max} = 0.5°$

(b) $\theta^0_{max} = 1°$

(c) $\theta^0_{max} = 2°$

(d) $\theta^0_{max} = 4°$

(e) $\theta^0_{max} = 6°$

(f) $\theta^0_{max} = 8°$

Figure 17: Response of $||h||$ with respect to the forcing with angle θ^0 with time t as parameter for the case with zero mean (θ^0_0= 0°), period T_{var}= 28 days with different amplitudes. The blue dashes denote a time interval of 2.5 days. Maximum values of $||h||$ are observed at different θ^0 for different θ^0_{max}.

5 Discussion and outlook

5.1 Choice of forcing periods

For the experiments with sinusoidally varying angles of wave incidence, the results of case2m were used. Case2m was the case in which a change to another constant angle of wave incidence was imposed after 150 days of normal wave incidence. Results showed that for a change from a constant wave forcing of 0° to 2°, an adaptation time t_a of approximately 15 days was found. In a sinusoid oscillation of θ^0 with an amplitude of 2° and a period of T_{var}, after every $T_{var}/4$, θ^0 changes 2°. Therefore the default value of the period $T_{var,d}$ was chosen to be approximately $4t_a$ with 56 days, because of the convenient fact that in the limit of faster oscillations, $T_{var,d}/2$ would be 28 days (monthly scale) and $T_{var,d}/8 = 7$days, the weekly scale on which crescentic bar patterns typically are observed [*Lippmann and Holman*, 1990]. The limit of slow variations was consistently chosen for $2T_{var,d}$ and $4T_{var,d}$ respectively for more theoretical insight.

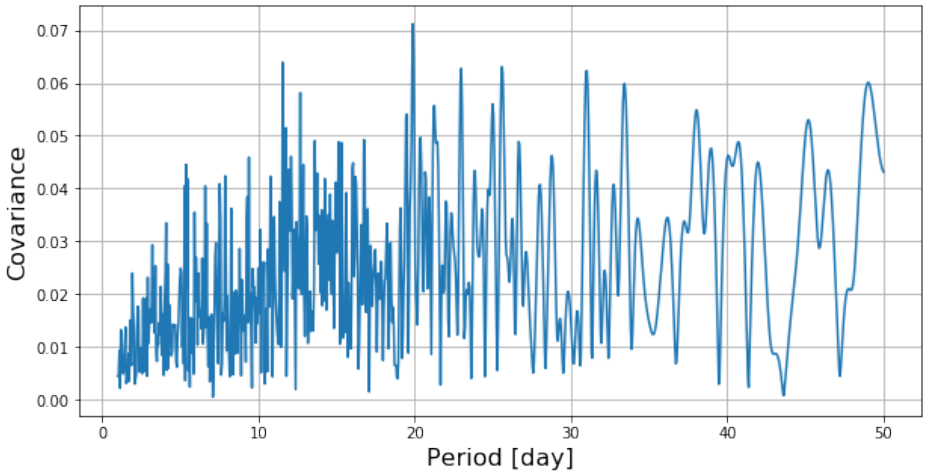

Figure 18: Covariance $(\alpha^2 + \beta^2)^{1/2}$ with α and β covariances of the cosine of the wave data and $\cos(\omega t)$, $\sin(\omega t)$ respectively, for different values of $T = 2\pi/\omega$. Here, ω is the angular frequency of measured angles of wave incidence. No significant peak is seen, so no typical recurrence period for events of certain wave angles is found.

In order to estimate whether the imposed time scales for the wave forcing are comparable to real situations, wave observational data for the North Sea have been used of the period 2003-2015. From this data, a selection has been made for wave directions belonging to wave heights of 0.5 m - 1.5 m and wave periods of 4 s - 8 s, since this range is chosen in the experiments.

The directions were weighted with sine and cosine functions and averaged over time, via

$$\alpha = \frac{1}{T}\int_0^T \cos(\theta)\cos(\omega t)dt, \tag{14}$$

$$\beta = \frac{1}{T}\int_0^T \cos(\theta)\sin(\omega t)dt, \tag{15}$$

where T here is the total time of the selected data and θ the wave directions from the dataset. From these coefficients, the covariance is calculated as $(\alpha^2 + \beta^2)^{1/2}$ for several values of ω, in order to investigate whether a certain ω corresponds to a typical recurrence frequency of certain wave directions θ. Results of this analysis for ω corresponding to periods up to $T = 2\pi/\omega = 50$ days are shown in figure 18, the range in time for which crescentic bar systems typically are observed. The maximal signal for $T = 20$ days is however not significant, so no typical recurrence period for events of certain wave angles is found. In order to obtain a more natural situation for simulating these systems, a real dataset as input can be used, including storm events and variations in the significant wave height and period, which in present study were held constant.

5.2 Differences with *Castelle and Ruessink* [2011]

The results of the experiments where the angle of wave incidence was varied around normal wave incidence with different periods T_{var} (case3T0) or different amplitudes θ^0_{max} (case3A0), can be compared the study of *Castelle and Ruessink* [2011], since in that study the same experiments were done- however with another model. In the present study, different results were found. First of all, in case3T0, the values for $||h||$, the mean deviation from the initial bed level, all lie around $||h||$ of the case with constant normal wave forcing. However, in *Castelle and Ruessink* [2011], $||h||$ is consistently lower for any periodical of wave forcing. In case3A0, the amplitude of the response in $||h||$| increases with larger forcing amplitudes θ^0_{max}. In *Castelle and Ruessink* [2011], only the mean of $||h||$ is affected.

To explain the differences, the differences in model setup have been identified. One difference is the bathymetry of both studies. Morfo55 does not take the swash zone into account (rigid coastline), where the model of *Castelle and Ruessink* [2011] has a variable coast line implemented. Moreover, their basic bathymetry is shallower than the specific profile of *Yu and Slinn* [2003], which is used in the present study. In order to match the profile of *Castelle and Ruessink* [2011] the most, equation (8) has been modified to

$$z^0_b(x) = -a_0 - \beta_2 x + a_2 \exp\left[-10(\frac{x - x_c}{x_c})^2\right], \tag{16}$$

with $a_0 = 0.25$ m in order to prevent model overflow at the coast and $\beta_2 = 0.02$ so that at $x = 500$ m, the depth is 10.6 m. In *Castelle and Ruessink* [2011] the bar is located 90 m from the level $z^0_b = 0$ m, which corresponds in equation (16) with $x_c = 77.5$ m and an amplitude of $a_2 = 1$ m so that the bar depth is equal to 0.8 m. The grid size has been set to 10 x 10 m, over the domain of 2000 m in y up to 500 m in x. The process was morphologically accelerated by a factor 45, γ was set to 20.4 to prevent model instabilities. However, when variations

in angle of wave incidence for several periods T_{var} were imposed with this bathymetry, no behaviour as in *Castelle and Ruessink* [2011] was found.

A second difference concerns the formulation of the sediment transport. In the present study the sediment formulation of *Soulsby* [1997] is employed, but in *Castelle and Ruessink* [2011] a formulation based on *Bailard* [1981] was used:

$$q_i = \alpha_{cr}(|u_{Bi}|^3 u_{Bi} - \gamma_{cr} u_b \frac{\partial h}{\partial x_i}), \tag{17}$$

with u_{Bi} the total velocity at the bottom (consisting of the mean current v_i at the bottom and u_b, the root-mean square orbital velocity at the bottom). In this expression, α_{cr} and γ_{cr} are called the stirring factor and the bed slope coefficient according to *Castelle and Ruessink* [2011], however, dimensions differ with their counterparts α and γ in the present study. Within equation (7), $[\alpha]$ = m and γ dimensionless, where $[\alpha_{cr}]$ =s^3 m^{-2}, $[\gamma_{cr}]$ = m^3 s^{-3} in order to match with the dimensions of q_i: m^2 s^{-1}. Within the formulation of *Soulsby* [1997], stirring coefficient α is variable or zero, depending on whether the total velocity at the bottom is more than a certain critical current velocity, u_{crit} [*Garnier*, 2006]. In the formulation of *Castelle and Ruessink* [2011], no critical velocity exists. Therefore it was checked whether the absence of u_{crit} would affect the dependence of the equilibrium value of $||h||$ for certain constant oblique angles of wave incidence θ^0, by turning $u_{crit} = 0$ within Morfo55. However a same dependence of $||h||$ on θ^0 was found as in figure 10 i.e., as in the case with non zero u_{crit}. First attempts to program the same sediment formulation of *Castelle and Ruessink* [2011] into Morfo55 have not been succeed.

A third difference between the two models concerns the description of waves. *Castelle and Ruessink* [2011] use the spectral wave model SWAN, which accounts for random waves with multiple frequencies and directions. In contrast, Morfo55 assumes waves to have a narrow spectrum with only one frequency and only one direction of propagation. However, implementation of the SWAN model into Morfo55 is not feasible.

To summarise, possible reasons for the different behaviour of the models are: the exclusion of the swash zone in Morfo55, the different sediment transport formulation and a different wave model. These reasons can be subject for research in the near future.

5.3 Physical interpretation for periodic forcing

To explain why in case of periodically changed angles of wave incidence θ^0, the response of the mean deviation from the initial bed level or mean height of the sandbars $||h||$ does not correspond with what is expected based on constant forcing, and moreover depends on the period T_{var} and amplitude θ^0_{max} of the varying forcing, it is important to consider the adjustment time scale t_a as determined in case2m (constant oblique wave angles on a mature sandbar pattern from normal wave incidence), with respect to T_{var}.
In particular, the behaviour of $||h||$ in case of varying wave angles around θ^0= 0° for several T_{var} (case3T0) is examined. Since in sinusoidal variation after $T_{var}/4$ the maximum is reached, τ, which is called is called the 'relative forcing period', is defined as $T_{var}/4t_a$. Here τ

explains the behaviour of the amplitude, the phase and the maximum value in the response of $||h||$|.

For small τ, the system and therefore $||h||$ is too inert to keep up the fast variations in forcing, hence the small amplitudes and the fact that the expected maximum based on constant oblique forcing is not reached in case of $T_{var} = 7$ days, for which $\tau \simeq 0.1$.
For large τ, so $T_{var} >> t_a$, the system is capable to adapt to the changing forcing and $||h||$ follows the changes in θ^0, as if at any time t a constant forcing-situation exists. However, in the particular cases of $T_{var} = 112$ days, 224 days, $||h|| - \theta^0$ plots of figure 14 do not show exactly the same behaviour for constant forcing. However, τ is probably not big enough for this limit to be fully applicable.
For intermediate values of τ, the period of the forcing variations is too long to have no influence at all, but the variations are fast enough to prevent the sandbars to fully adapt. Sandbars continue to grow even when the forcing is changed in the mean time, and $||h||$ becomes higher than at constant forcing. In other words, phase differences occur between the periodical behaviour in $||h||$ and the forcing for $T_{var} = 28$ days, 56 days: for certain periodical forcing, observed values of $||h||$ do not correspond to the actual forcing on specific time t, but correspond to the forcing of earlier in phase.
This role of τ implies that depending the specific proportionality between the ability of adapting and the rate of change of the forcing, not all bar height controlling mechanisms come to light as actual manifestations of certain bar heights, or with a certain delay.

For case3T2 (on average wave directions of 2°), the same physical interpretation can be found as for case3T0, since observations in figure 19 show the same behaviour as case3T0 in figure 14. For case3T4, observations were different. Also for amplitude variations, more research is needed, since only for certain combinations of mean variations and amplitudes, the system act as one would expect based on the value of τ.

Besides, this interpretation does not explain why even for the lowest or highest values of T_{var}, the mean of the variation in $||h||$ is different from the value of $||h||$ in case of constant forcing and that the mean differs for different values of T_{var}. This might be ascribed to the nonlinearity of the terms that cause growth or decay of $||h||$, which also can be subject for further research.

5.4 Model limitations

As a remark to all of the above discussion on results, one has to bear in mind that all results have been obtained by using a model, which has several limitations as *Garnier* [2006] has pointed out, some of these already mentioned in section 5.2. In addition to these, the model is highly dependent on the chosen value of γ_b and γ, for slightly other choices the model became unstable. Refraction of wave incidence due to the new bed level topography was not taken into account as well. Finally, the existence of a certain critical angle for above which no growth of sandbars is observed, is not consistent with observations [*Garnier et al.*, 2008].

6 Conclusions

The main objective was to investigate the behaviour of the periodically changes in angle of wave incidence not only with zero mean, but also with non zero mean, in order to answer the research question.

For periodically variations in wave angle with zero mean, other features of the mean height of the sandbars were found than in the study of *Castelle and Ruessink* [2011]. Since several possible reasons have been investigated, the different behaviour of the two models might be described to the exclusion of the swash zone in Morfo55, the difference in sediment description and the difference in the used wave model.

For periodically variations in wave angle, bars migrate in phase with the time-variant forcing, but their mean height behaves differently than expected based on findings for constant wave forcing. Mainly for variations with zero mean, it is found that the ratio of the time the system needs to adapt to new types of wave forcing and the rate of change of the wave forcing can explain most of these differences. For non zero mean, the specific behaviour is more complex than for mean normal wave incidence and in some cases the expected behaviour based on the ratio of adaptation time and forcing time was not observed, for which an explanation is beyond the scope of this research.

References

Bailard, J., An energetics total load sediment transport model for a plane sloping beach, *Journal of Geophysical Research*, *86*, 10,93810,954, 1981.

Caballeria, M., G. Coco, A. Falqués, and D. A. Huntley, Self-organization mechanisms for the formation of nearshore crescentic and transverse sand bars, *Journal of Fluid Mechanics*, *465*, 379410, 2002.

Castelle, B., and B. Ruessink, Modeling formation and subsequent nonlinear evolution of rip channels: Timevarying versus timeinvariant wave forcing, *Journal of Geophysical Research*, *116*, 2011.

CoastalWiki, Stability models, `http://www.coastalwiki.org/wiki/Stability_models`, [Online; accessed 20-April-2018], 2017.

Davis Jr., R., and D. M. Fitzgerald, *Beaches and Coasts*, 1 ed., Blackwell Science Ltd, Malden, U. S. A., 2004.

Garnier, R., Nonlinear modelling of surf zone morphodynamical instabilities, Ph.D. thesis, Universitat Politècnica de Catalunya, Barcelona, 2006.

Garnier, R., D. Calvete, A. Falqués, and M. Caballeria, Generation and nonlinear evolution of shore-oblique/transverse sand bars, *Journal of Fluid Mechanics*, *567*, 327360, 2006.

Garnier, R., D. Calvete, A. Falqués, and N. Dodd, Modelling the formation and the long-term behavior of rip channel systems from the deformation of a longshore bar, *Journal of Geophysical Research*, *113*, 2008.

Garnier, R., N. Dodd, A. Falqués, and D. Calvete, Mechanisms controlling crescentic bar amplitude, *Journal of Geophysical Research*, *115*, 2010.

Garnier, R., A. Falqués, D. Calvete, and F. R. J. Thiébot, A mechanism for sandbar straightening by oblique wave incidence, *Geophysical Research Letters*, *40*, 2013.

Horikawa, K., *Nearshore Dynamics and Coastal Processes*, University of Tokio Press., Tokio, Japan, 1988.

Leatherman, S. P., Undertow, rip current, and riptide, *Journal of Coastal Research*, *28*, 3–5, 2012.

Lippmann, T. C., and R. A. Holman, The spatial and temporal variability of sand bar morphology, *Journal of Geophysical Research*, *95*, 575–590, 1990.

Mei, C., *The Applied Dynamics of Ocean Surface Waves, Advanced Series on Ocean Engineering*, World Scientific, Singapore, 1989.

Ribas, F., A. Falqués, H. E. de Swart, N. Dodd, R. Garnier, and D. Calvete, Understanding coastal morphodynamic patterns from depth-averaged sediment concentration, *Review of Geophysics*, *53*, doi:10.1002/2014RG000457, 2015.

Rutten, J., B. Dubarbier, T. Price, and B. C. G. Ruessink, Crescentic bar patterns along curved coaststst: observations and modelling, *Coastal Dynamics*, p. 18321842, 2017.

Short, A. D., *Handbook of Beach and Shoreface Morphodynamics*, Wiley, Chichester, U. K., 1999.

Soulsby, R. L., *Dynamics of Marine Sands*, Thomas Telford, London, 1997.

Thornton, B., and R. T. Guza, Transformation of wave height distribution, *Journal of Geophysical Research*, *88*, 1983.

Van Enckevort, I. M. J., and B. G. Ruessink, Video observations of nearshore bar behaviour. part 2: alongshore non-uniform variability, *Continental Shelf Research*, *23*, 512–532, 2003.

Vis-Star, N. C., H. de Swart, and D. Calvete, Patch behaviour and predictability properties of modelled finite-amplitude sand ridges on the inner shelf, *Nonlinear Processes in Geophysics*, *15*, 943955, 2008.

Wright, L. D., and A. D. Short, Morphodynamic variability of surf zones and beaches: A synthesis, *Marine Geology*, *56*, 93–118, 1984.

Yu, J., and D. N. Slinn, Effects of wave-current interaction on rip currents, *Journal of Geophysical Research*, *108*, 2003.

A Figures

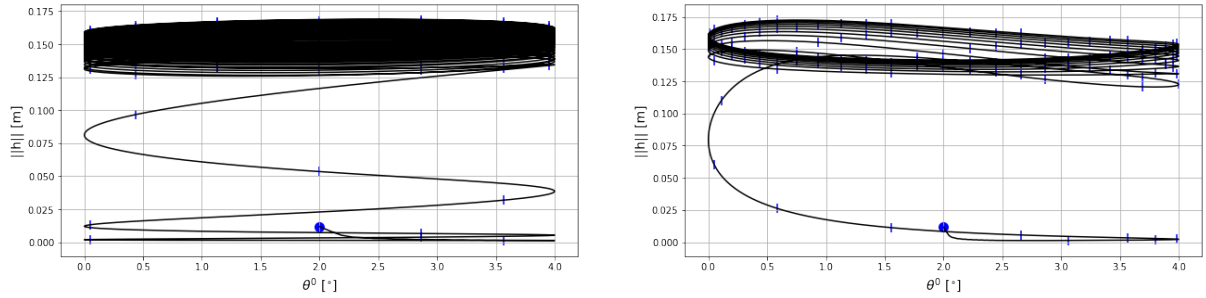

(a) $T_{var} = 7$ days

(b) $T_{var} = 28$ days

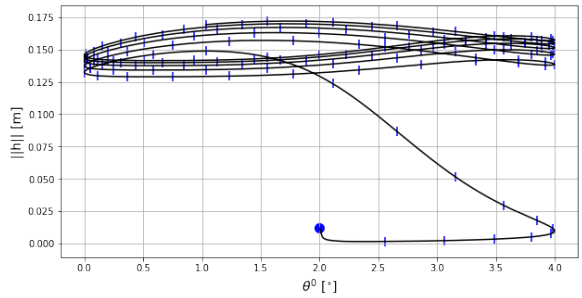

(c) $T_{var} = 56$ days

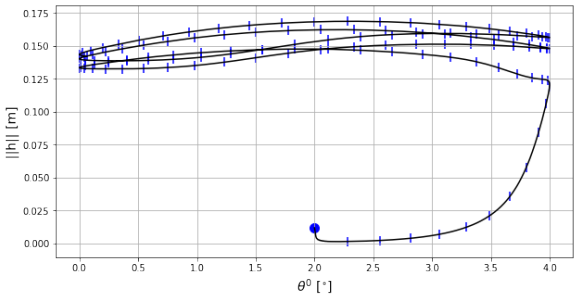

(d) $T_{var} = 112$ days

Figure 19: Response of $||h||$, the mean deviation from the initial bed level, with respect to the forcing with angle θ^0 with time t as parameter for non zero mean (θ^0_0= 2°, amplitude θ^0_{max}= 2°) and different forcing periods. The blue dashes denote a time interval of 2.5 days.

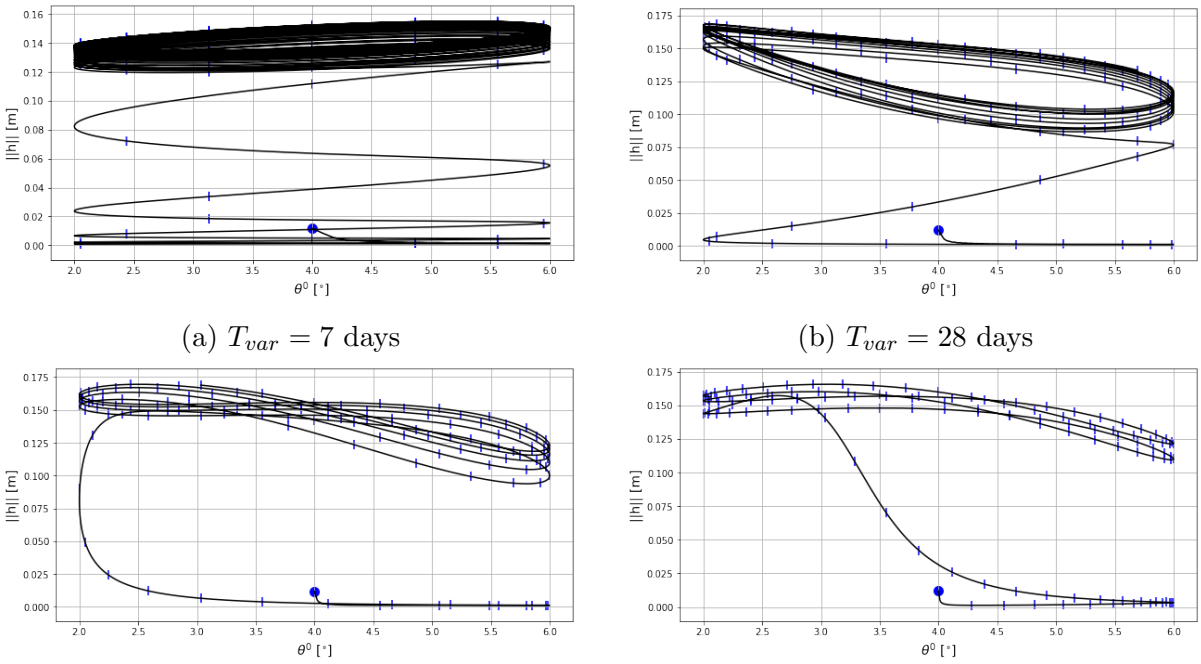

(a) $T_{var} = 7$ days

(b) $T_{var} = 28$ days

(c) $T_{var} = 56$ days

(d) $T_{var} = 112$ days

Figure 20: Response of $||h||$ with respect to the forcing with angle θ^0 with time t as parameter for non zero mean (θ^0_0= 4°, amplitude θ^0_{max}= 2°) and different forcing periods. The blue dashes denote a time interval of 2.5 days.

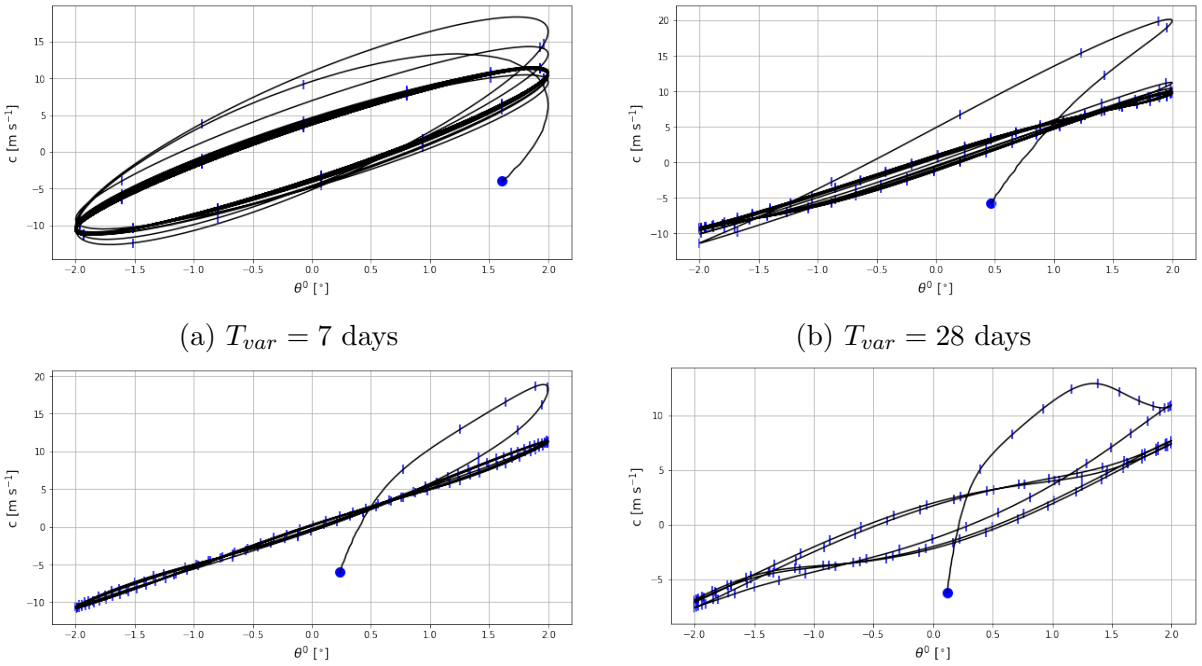

(a) $T_{var} = 7$ days

(b) $T_{var} = 28$ days

(c) $T_{var} = 56$ days

(d) $T_{var} = 112$ days

Figure 21: Response of longshore current c with respect to the forcing with angle θ^0 with time t as parameter for the case with zero mean ($\theta^0_0 = 0°$, amplitude $\theta^0_{max} = 2°$) and different forcing periods. The blue dashes denote a time interval of 2.5 days. The starting point of these figures is at $t = 2.5$ days and is denoted with the blue dot.

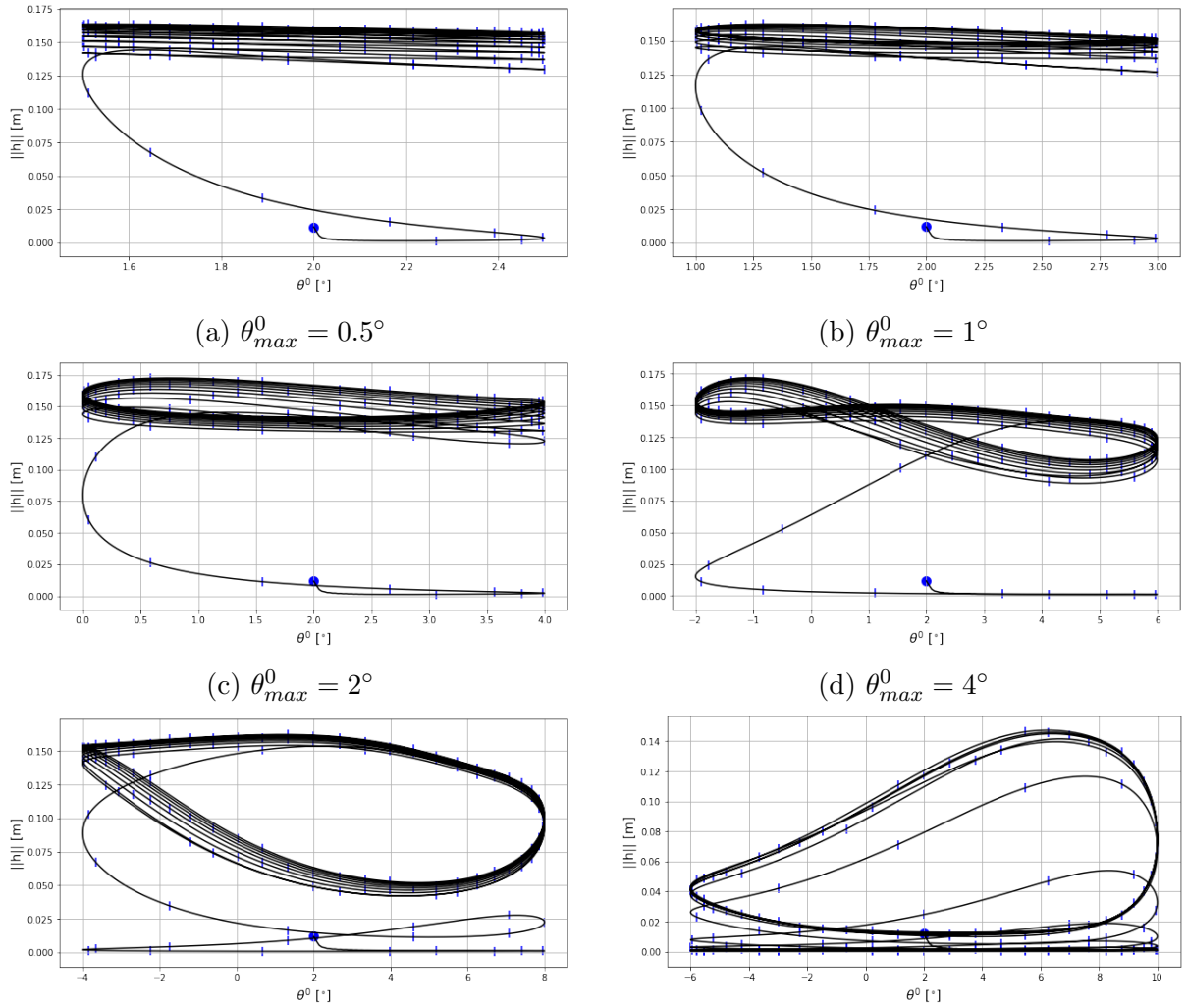

(a) $\theta^0_{max} = 0.5°$

(b) $\theta^0_{max} = 1°$

(c) $\theta^0_{max} = 2°$

(d) $\theta^0_{max} = 4°$

(e) $\theta^0_{max} = 6°$

(f) $\theta^0_{max} = 8°$

Figure 22: Response of $||h||$ with respect to the forcing with angle θ^0 with time t as parameter for non zero mean (θ^0_0= 2°, period T_{var}= 28 days) with different amplitudes. The blue dashes denote a time interval of 2.5 days

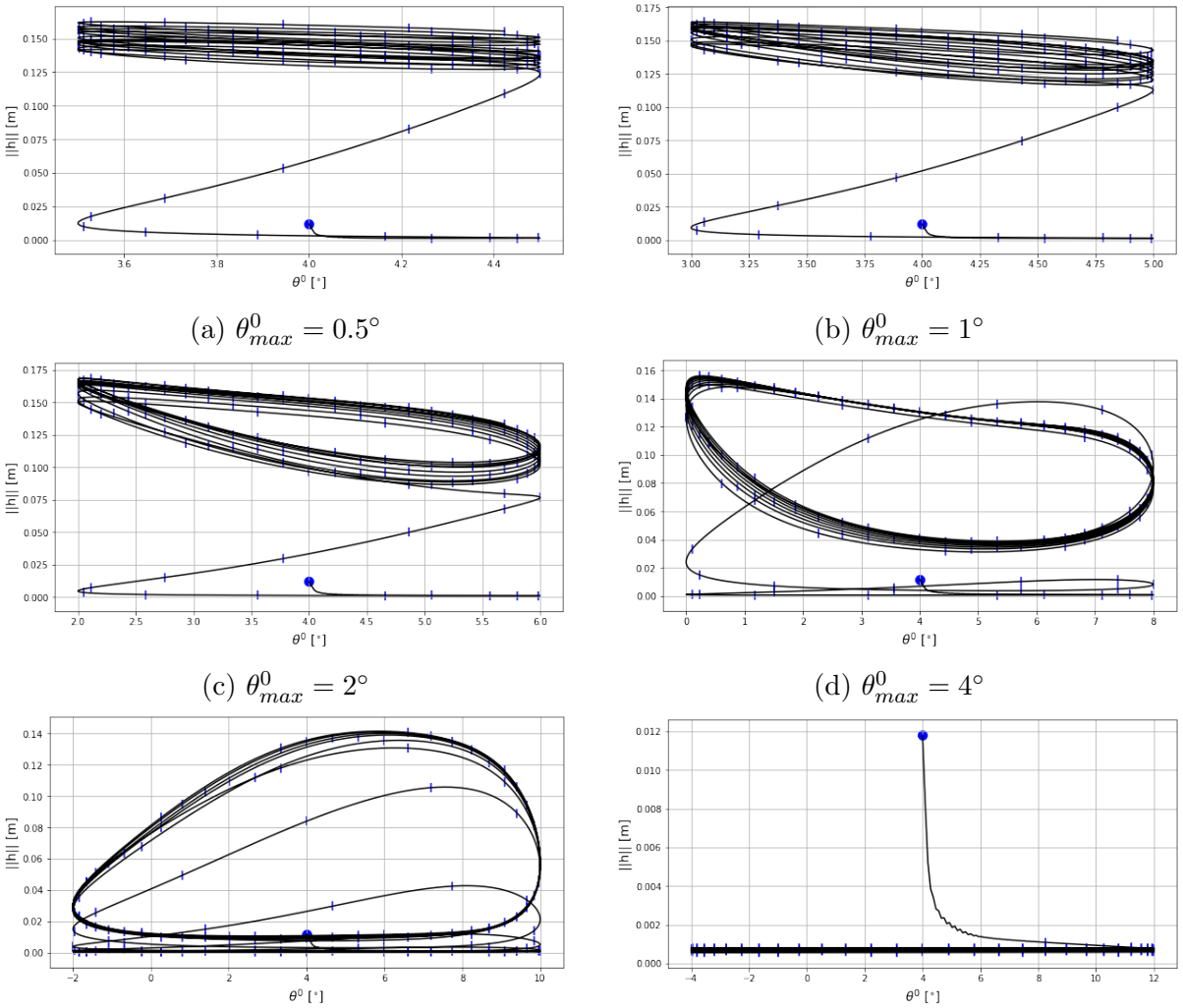

(a) $\theta^0_{max} = 0.5°$

(b) $\theta^0_{max} = 1°$

(c) $\theta^0_{max} = 2°$

(d) $\theta^0_{max} = 4°$

(e) $\theta^0_{max} = 6°$

(f) $\theta^0_{max} = 8°$

Figure 23: Response of $||h||$ with respect to the forcing with angle θ^0 with time t as parameter for non zero mean (θ^0_0= 4°, period T_{var}= 28 days) with different amplitudes. The blue dashes denote a time interval of 2.5 days.